



# Baseline brain function in the preadolescents of the ABCD Study

**The Adolescent Brain Cognitive Development (ABCD) Study<sup>\*</sup> is a 10-year longitudinal study of children recruited at ages 9 and 10. A battery of neuroimaging tasks are administered biennially to track neurodevelopment and identify individual differences in brain function. This study reports activation patterns from functional MRI (fMRI) tasks completed at baseline, which were designed to measure cognitive impulse control with a stop signal task (SST;  $N = 5,547$ ), reward anticipation and receipt with a monetary incentive delay (MID) task ( $N = 6,657$ ) and working memory and emotion reactivity with an emotional N-back (EN-back) task ( $N = 6,009$ ). Further, we report the spatial reproducibility of activation patterns by assessing between-group vertex/voxelwise correlations of blood oxygen level-dependent (BOLD) activation. Analyses reveal robust brain activations that are consistent with the published literature, vary across fMRI tasks/contrasts and slightly correlate with individual behavioral performance on the tasks. These results establish the preadolescent brain function baseline, guide interpretation of cross-sectional analyses and will enable the investigation of longitudinal changes during adolescent development.**

The ABCD Study<sup>\*</sup> aims to characterize adolescent development and evaluate many influences that might shape developmental trajectories. While numerous factors are plausibly associated with neurodevelopment (for example, nutrition, sleep, exercise, head injuries and substance use), we have a limited understanding of the magnitude of their effects, their interactions with one another and the moderating influences of other risk or resilience factors. The longitudinal ABCD Study ([www.ABCDstudy.org](http://www.ABCDstudy.org)) aims to address these matters with an especially large, demographically diverse sample that is richly characterized with extensive phenotyping and genotyping. It realizes an open science model through which data are fully shared with the research community.

This manuscript describes the ABCD baseline assessment of brain function in 9- and 10-year-old participants. As the bulk of the human neuroimaging literature has focused on adult functioning, less is known about brain function in childhood and, particularly, in preadolescent children. Neurodevelopment from ages 10 to 20 is, however, of particular interest as these ages are associated with notable brain, cognitive and emotional maturation and the emergence of many prevalent mental health disorders<sup>1</sup>. Consequently, there is great interest in understanding the etiology and neurobiology of psychological processes thought to be risk factors for the development of mental and physical health challenges, including cognitive control, reward, working memory and social/emotional function.

Cognitive control is often assessed using inhibitory tasks, such as the SST, in which a motor response must be countermanded<sup>2</sup>. Inhibitory tasks, including the SST, are known to elicit activation in the dorsal anterior cingulate (dACC), inferior frontal gyrus (IFG), dorsolateral prefrontal cortex (dlPFC) and insula<sup>3</sup>. Studies of these processes in children and adolescents have typically found similar regional activation during inhibitory tasks<sup>4</sup>. Consistent results have been found for fMRI and electroencephalogram (EEG) studies showing that from childhood to adolescence there is an increase in brain activity in the dACC<sup>5</sup>, which corresponds to improved inhibitory control<sup>6</sup>. However, this pattern may not be consistent across the brain, as there have been mixed findings regarding whether activation in the dlPFC and IFG increases with age and improved inhibitory control<sup>3–7</sup>, with more recent findings suggesting that activation

in the prefrontal cortex may decrease throughout adolescence, paralleling improved inhibitory control<sup>4,8,9</sup>.

Functional neuroimaging investigations of working memory also demonstrate substantial concordance between adults and children in neural responses as well as some notable differences<sup>10–12</sup>. A recent meta-analysis of verbal and visuospatial N-back tasks (in which one indicates if a currently presented stimulus is the same as a stimulus presented  $n$  items earlier in a serial stream of stimuli) found that adults and children show consistent patterns of activation in the dlPFC, posterior parietal cortex (PPC), supplementary motor area (SMA) and insula<sup>10</sup>. However, similar to the SST, regional levels of activation during the N-back task have been shown to differ between children and adults, mirroring improvements in working memory ability<sup>13–15</sup>. In the largest study to date to examine change in functional activation during the N-back task across adolescence ( $N = 951$ ), Satterthwaite et al.<sup>13</sup> found increases in activation in the dlPFC, SMA and PPC from ages 8 to 22. Interestingly, they also found decreased activation in the default mode network (DMN), suggesting improved segregation of the cognitive control and DMN regions with advancing age and improved performance on the task. One study using a subset from the ABCD baseline assessment found that frontoparietal activity during the 2-back (relative to 0-back) task relates to working memory performance measured out of the scanner using the list sort task, suggesting that brain activity during the N-back task functions as a general index of working memory ability<sup>16</sup>.

Importantly, by varying the stimuli, psychological tasks can also implicitly probe social and emotional processes. A recent meta-analysis of affective working memory tasks in adolescents and adults found that there was little effect on working memory performance when using affective stimuli, and that the differences that were observed were more concentrated among older adults (Schweizer et al.<sup>17</sup>; 165 studies,  $N = 7,433$ ). However, this analysis did find differences in brain activation associated with affective working memory stimuli (33 fMRI studies,  $n = 683$ ), with affective stimuli more likely to elicit activation in the ventromedial prefrontal cortex (vmPFC), amygdala, temporal cortex and occipital cortex. While this analysis did not examine emotional faces specifically, studies of emotional faces were included, likely explaining the

A full list of affiliations appears at the end of the paper.

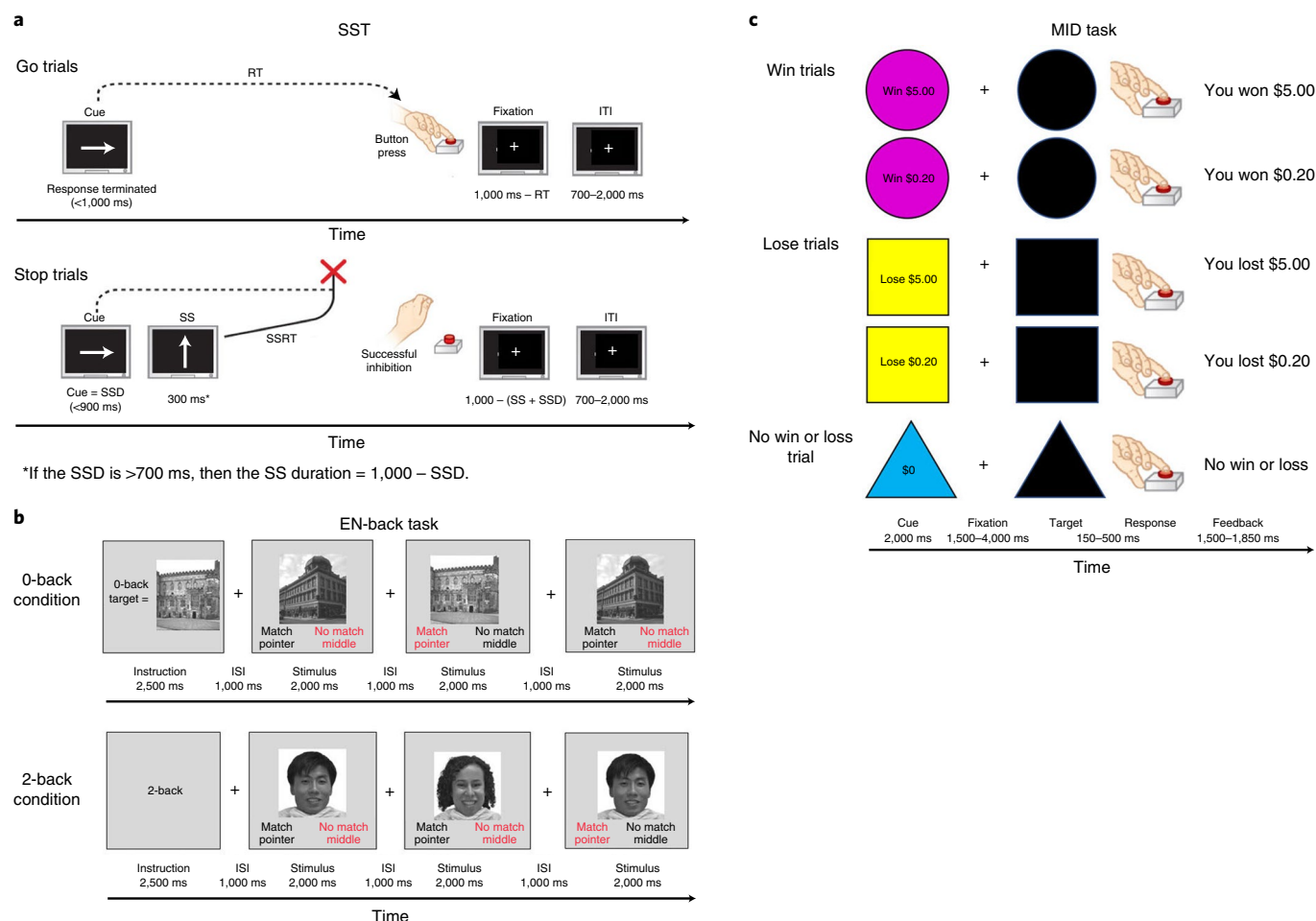


**Fig. 1 | fMRI task designs in the ABCD study. a–c.** Schematics of the SST (**a**), the EN-back task (**b**) and the MID task (**c**). Schematics reproduced from ref. <sup>51</sup>, under a CCB 4 license; ISI, interstimulus interval; ITI, intertrial interval; RT, reaction time; SS, stop signal; SSD, stop signal delay; SSRT, stop signal reaction time.

observed temporal/occipital activations. In other studies, working memory tasks using facial stimuli have been found to elicit differential patterns of activation in the temporal/occipital cortices, specifically in the fusiform face area (FFA) and occipital face area (OFA)<sup>18,19</sup>. A recent large study by Fuhrman et al.<sup>20</sup> ( $N=661$ ) found that the ability to distinguish faces is still developing until age 16, confirming prior smaller studies<sup>21</sup>. Scherf et al.<sup>22</sup> found that adolescents aged 11–14 years old showed similar but attenuated patterns of face-related activation compared to adults. In one of the largest studies of adolescents to date ( $N=1,100$ ), Tahmasebi et al.<sup>23</sup> found similar regions activated by facial stimuli in adolescents aged 13–15 years old, including the FFA, OFA and superior temporal sulcus (STS). However, this study included neither younger children nor older adult comparison groups. While the primary regions elicited by facial recognition tasks are likely similar throughout development, there is evidence that activation in core facial recognition regions (that is, the FFA, OFA and STS) increases in response to these tasks throughout development starting at age 7 to 8 (ref. <sup>24</sup>). Additionally, work by Kadosh et al.<sup>25</sup> found that complementary regions supporting the primary facial recognition regions change throughout development ( $N=42$ ). When considering young children (aged 5–8 years old), Scherf et al.<sup>26</sup> found that children did not demonstrate these characteristic patterns of activation to faces at all, lacking activation in the FFA, OFA and STS ( $N=30$ ), although their activation to place stimuli in the parahippocampal area was similar

to that of adults. Indeed, several other studies concluded that the FFA is not consistently activated in children under the age of 8 (for review, see Scherf et al.<sup>22</sup>).

With regard to reward-related processes, such as reward anticipation and receipt, many studies have suggested similar task-related fMRI activation in children and adolescents aged 12–17 as in adults, with a network of reward anticipation regions, including the ventral and dorsal striatum, the insula, SMA, premotor cortex, thalamus and amygdala, and a network of reward receipt regions, including the ventral striatum (VS), amygdala, vmPFC and posterior cingulate cortex (PCC)<sup>27–29</sup>.

Overall, investigations into these key neurocognitive processes suggest qualitatively similar patterns of activation in children and adults with some inconsistencies across studies, likely due, in part, to small samples of convenience. Indeed, low reproducibility in psychological and clinical neuroimaging studies due to small sample sizes is now acknowledged to be a critical concern in the field<sup>30–32</sup>. While Thirion et al.<sup>33</sup> suggested that 20 or more participants are required for reliable task-based fMRI inferences, Turner et al.<sup>34</sup> recently pointed out using the large fMRI dataset of the Human Connectome Project (HCP)<sup>35</sup> that such recommendations are outdated. Indeed, Turner et al. report that even datasets with 100 or more participants can produce results that do not replicate, suggesting that larger sample sizes are necessary for task-based fMRI<sup>34</sup>.

**Table 1 | Inclusion criteria in the task fMRI analyses and number of participants remaining after each step of exclusions**

Criteria\task	EN-back	SST	MID
Total number scanned participants	10,189	10,294	10,385
Two runs that passed MRI quality control	8,981	9,035	9,140
Data available excluding Philips scans	8,163	8,140	8,201
Mutual vertex and voxel data availability	7,969	7,288	7,427
Motion censoring (mean FD < 0.9 mm)	7,680	7,000	7,239
d.f. across runs >200	7,680	7,000	7,225
Beta weights outlier detection	6,666	6,995	7,214
Passed behavioral performance QC	6,085	5,116	6,753
No missing covariates	6,009	5,547	6,657

Covariates include age, sex, education, puberty, race, family and scanner ID. FD, framewise displacement; QC, quality control.

Here, we report cortical and subcortical analyses of the ABCD task fMRI battery assessing response inhibition, working memory and reward processing assayed via the SST, EN-back task and MID task (Fig. 1), respectively, at the study's first acquisition time point. We focus on (1) the patterns and magnitude of brain activity as predicted by prior research in adolescent samples; (2) the reproducibility of activation patterns, including an assessment of group-level reproducibility as a function of sample size; and (3) the relationships between activation magnitudes and individual differences in task abilities during response inhibition and working memory. We hypothesized that the three fMRI tasks would show robust patterns of activation consistent with those identified in prior studies in children mentioned in the literature review above, including cortico-striatal activations associated with motor response inhibition<sup>3,4</sup>, frontoparietal activation associated with working memory performance<sup>10,36</sup> and dopaminergically rich subcortical regions associated with reward processes<sup>27–29</sup>. Additionally, we hypothesized that patterns of associations between task performance and task activation would mirror activation patterns, as has been found in prior literature. Further, we hypothesized that reproducible group-level activation maps would likely differ among tasks (being biggest on the block design primary EN-back contrasts) and likely require more participants than are included in typical neuroimaging studies to reproduce effects.

The analyses that are reported were designed to provide a largely descriptive account of the patterns of activation present in the ABCD sample. For instance, we report all analyses in effect sizes and do not threshold by statistical significance. The goal of the present paper is to provide a baseline reference (task activation magnitudes, sensitivity to individual differences in performance and reproducibility) for researchers using the ABCD task fMRI data to address their questions of interest regarding adolescent brain development.

## Results

After applying the exclusion criteria (see Table 1 and Methods for details), the resulting sample sizes and demographics among the fMRI tasks were as follows: SST ( $N = 5,547$ , mean age =  $9.96 \pm 0.63$ , 49.82% male), EN-back ( $N = 6,009$ , mean age =  $9.96 \pm 0.63$ , 50.77% male) and MID ( $N = 6,657$ , mean age =  $9.95 \pm 0.63$ , 50.43% males). Table 2 presents the demographic composition of samples that were included and excluded from the current study (see Methods for details).

**Individual behavior performance measures and task fMRI beta weights.** Performance on the SST was in the anticipated range (mean (s.d.), SSRT = 302.6 (67.1) and Go RT = 529.9 (77.4)), with a rate of

correct inhibitions of 51.4% (0.06). The distributions for EN-back  $D'$  values were as expected, with children performing better on the 0-back task ( $D' = 2.51$  (0.9)) than on the 2-back task ( $D' = 2.0$  (0.3);  $P < 0.001$ ).  $D'$  mean (s.d.) values from the post-scan recognition memory test were 0.94 (0.63) for happy faces, 0.92 (0.63) for fearful faces, 0.85 (0.61) for neutral faces and 1.34 (0.82) for places. The distributions of SSRT and  $D'$  behavioral performance measures are shown in Fig. 2. Paralleling the individual differences in performance, task activations in relevant task regions of interest (ROIs) also show large interindividual variation; Fig. 2 shows the distribution of average local maxima beta weights within task-specific regions known to be involved in SST (Fig. 2d,e), EN-back (Fig. 2f) and MID (Fig. 2g) tasks. An analysis of covariance (ANCOVA) assessing the correlation between  $D'$  values from the post-scan recognition memory test and EN-back beta weights in the bilateral dlPFC showed significant associations across contrasts and conditions, yet with small correlation coefficients, with the most important association observed between the happy faces condition and the 2-back versus 0-back contrast ( $P = 0.0001$  and  $r = 0.17$ ).

**Task activation Cohen's  $d$ .** Cortical and subcortical Cohen's  $d$  maps of contrasts for each task are represented in composite Figs. 3a,b, 4a,b, 5a,b and 6a,b. In addition, static and three-dimensional (3D) dynamic views of both thresholded and unthresholded Cohen's  $d$  maps are available online (download required to display the dynamic maps) at [https://drive.google.com/drive/folders/1VPnY8SS68JYis-AI-mt8\\_BJqc4r6GD5D](https://drive.google.com/drive/folders/1VPnY8SS68JYis-AI-mt8_BJqc4r6GD5D). Task fMRI activation maps generated from the ABCD dataset are provided in Supplementary Data 1 for the research community to use as task fMRI activation templates in children, are available online as manuscript files and can be downloaded as high-resolution MGZ images.

As shown in Fig. 3, the SST showed robust activation for both correct Stop versus correct Go and incorrect Stop versus correct Go conditions in multiple frontoparietal, temporal, insular and occipital regions of the cortex. Key nodes of the response inhibition circuitry, such as the IFG, dACC, pre-SMA and, subcortically, the putamen and caudate, were activated. Deactivations were observed in the left postcentral somato-sensorimotor cortex (presumably reflecting the motor response that is present on Go trials and absent on successful inhibitions) and in DMN centers, including the precuneus and vmPFC.

As shown in Fig. 4, the 0-back versus fixation and 2-back versus fixation contrasts of the EN-back task produced widespread robust activation in bilateral regions, including parts of the superior, middle and inferior frontal gyri, the inferior parietal lobule, the dACC/SMA, the precentral gyrus and the occipital pole. Substantial deactivations were also observed within a number of bilateral regions, including the precentral and postcentral gyri, superior parietal lobule, lingual gyrus, precuneus/PCC, the rostral ACC/vmPFC and the posterior insula. The 2-back versus 0-back subtraction showed more circumscribed activity in the middle and superior frontal gyri, inferior parietal gyrus, precuneus and dACC as well as focal deactivations in the vmPFC/rostral ACC, PCC, precentral gyrus and posterior insula. As expected, the faces versus places contrast revealed dissociable activations; face stimuli produced elevated activation in the FFA, OFA and bilateral amygdalae, while place stimuli robustly activated large portions of the occipital cortex in addition to hippocampal and parahippocampal regions. The negative and positive faces contrasted to neutral faces (Fig. 5) showed reduced activations compared to the other contrasts, with the most notable effects being activation in the amygdalae for negative versus neutral faces and deactivation in bilateral putamen for positive versus neutral faces.

As shown in Fig. 6, anticipation of potential wins and losses on the MID task produced largely similar patterns of activation in parts of the ACC, precentral gyrus, inferior parietal lobule and frontal and occipital gyri as well as in the bilateral anterior insula (AI) and

**Table 2 | Demographics for all participants included and excluded from the analyses**

Measure	EN-back, included (N = 6,009)	EN-back, excluded (N = 4,353)	Statistics <sup>a</sup>	SST, included (N = 5,547)	SST, excluded (N = 4,815)	Statistics <sup>a</sup>	MID, included (N = 6,657)	MID, excluded (N = 3,705)	Statistics <sup>a</sup>
<b>Sex</b>									
Male	3,051	2,378	$\chi^2$ (1, N = 10,361) = 15.14, P < 0.001	2,767	2,666	$\chi^2$ (1, N = 10,362) = 30.63, P < 0.001	3,357	2,073	$\chi^2$ (1, N = 10,362) = 28.98, P < 0.001
Female	2,958	1,974	Cramer's V = -0.04	2,780	2,149	Cramer's V = -0.05	3,300	1,632	Cramer's V = -0.05
No answer		1							
<b>Age</b> (years; mean $\pm$ s.d.)	9.96 $\pm$ 0.63	9.84 $\pm$ 0.61		9.96 $\pm$ 0.63	9.86 $\pm$ 0.62		9.95 $\pm$ 0.63	9.85 $\pm$ 0.61	
9	2,929	2,529	t(9,520.93) = 10.31, P < 0.001	2,731	2,713	t(10,361) = 298.92, P < 0.001	3,335	2,123	t(7,814.1) = 8.14, P < 0.001
10	3,080	1,824		2,816	2,102		3,322	1,582	
<b>Race/ethnicity</b>									
White	3,428	1,884	$\chi^2$ (4, N = 10,345) = 262.28, P < 0.001	3,172	2,148	$\chi^2$ (4, N = 10,360) = 206.05, P < 0.001	3,680	1,632	$\chi^2$ (4, N = 10,345) = 185.56, P < 0.001
Black	685	926	Cramer's V = 0.16	657	957	Cramer's V = 0.14	826	785	Cramer's V = 0.13
Hispanic/Latino	1,170	920		1,069	1,023		1,347	743	
Asian	121	93		114	100		129	85	
Other	605	513		535	585		675	443	
No answer		17			2			17	
<b>Highest household education</b>									
<High school diploma	192	288	$\chi^2$ (4, N = 10,345) = 236.65, P < 0.001	182	298	$\chi^2$ (4, N = 10,348) = 170.76, P < 0.001	244	236	$\chi^2$ (4, N = 10,345) = 143.87, P < 0.001
High school diploma/GED	445	545	Cramer's V = 0.15	437	553	Cramer's V = 0.13	553	437	Cramer's V = 0.12
Some college	1,493	1,293		1,359	1,429		1,671	1,115	
Bachelors	1,650	1,003		1,517	1,136		1,795	858	
Postgraduate degree	2,221	1,215		2,044	1,393		2,386	1,050	
No answer	8	9		8	6		8	9	
<b>Household income per year (US\$)</b>									
<50,000	1,395	1,475	$\chi^2$ (2, N = 9,502) = 203.70, P < 0.001	1,285	1,585	$\chi^2$ (2, N = 9,503) = 168.93, P < 0.001	1,613	1,257	$\chi^2$ (2, N = 9,502) = 155.41, P < 0.001
50,000-100,000	1,620	1,084	Cramer's V = 0.15	1,485	1,220	Cramer's V = 0.13	1,774	930	Cramer's V = 0.13
>100,000	2,584	1,344		2,382	1,546		2,780	1,148	
No answer	229	205		224	209		250	189	
Participant did not know	181	245		171	255		240	181	
<b>Handedness</b>									
Right	4,849	3,401	$\chi^2$ (2, N = 10,362) = 11.08, P = 0.004	4,497	3,753	$\chi^2$ (2, N = 10,362) = 16.01, P < 0.001	5,379	2,871	$\chi^2$ (2, N = 10,362) = 19.85, P < 0.001
Left	418	325	Cramer's V = 0.03	377	366	Cramer's V = 0.04	470	273	Cramer's V = 0.04
Ambedextrous	742	627		673	696		808	561	

GED, graduate equivalency degree <sup>a</sup>Age, t-test between participants that were included in the analysis and participants that were excluded from the analysis; all other variables, Pearson  $\chi^2$  test.

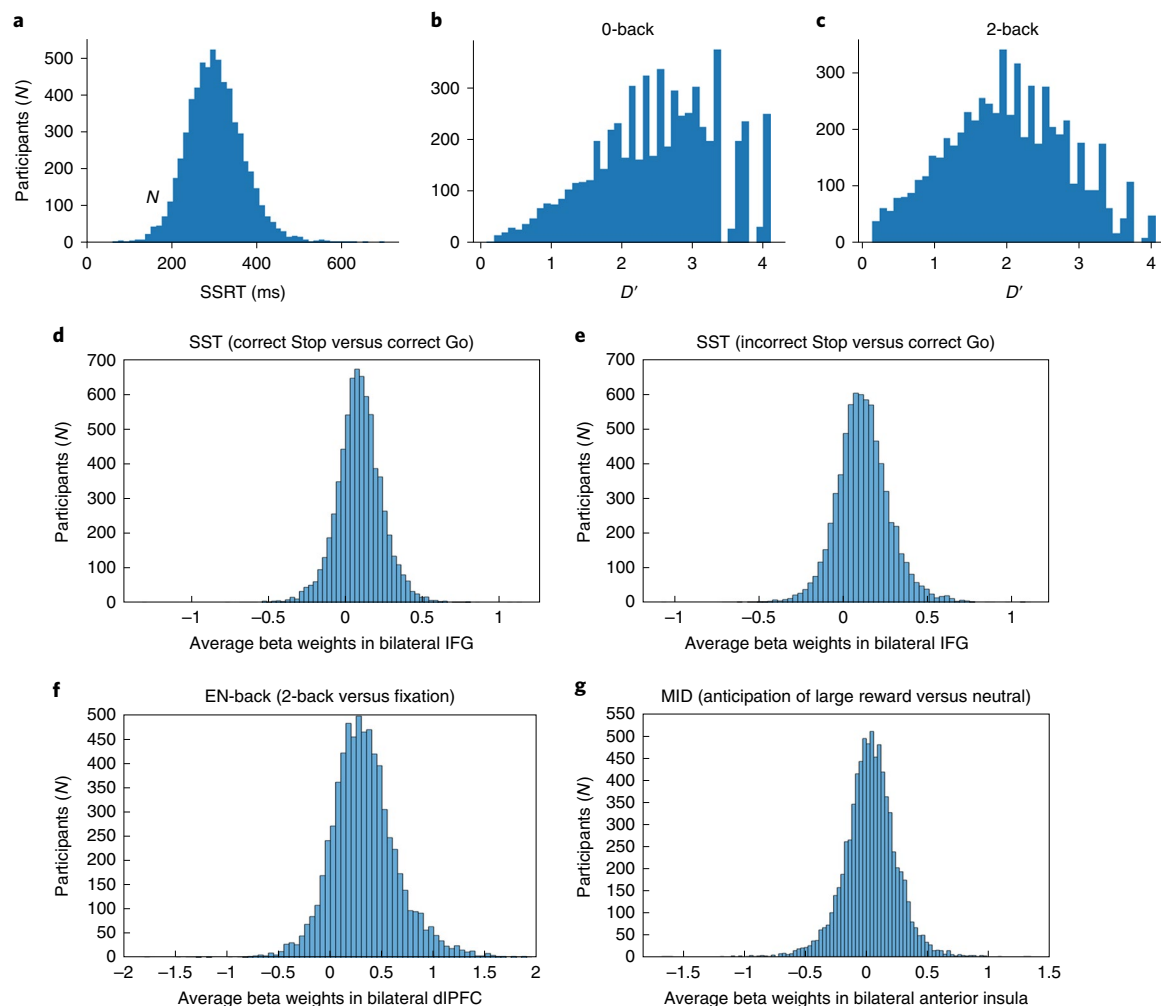


**Fig. 2 | The distribution of behavioral performance measures and beta weights in the sample. a–c,** Distribution of behavioral performance. Top: distribution of SSRT (**a**), 0-back  $D'$  (**b**) and 2-back  $D'$  (**c**) behavioral performance measures in the sample. **d–g,** Distribution of beta weights. Bottom: distribution of average local maxima beta weights in the sample within task-specific regions commonly known to be involved in SST (**d,e**), EN-back (**f**) and MID (**g**) tasks; SST,  $N=5,547$ ; EN-back,  $N=6,009$ ; MID,  $N=6,657$ .

extensive subcortical regions. The feedback contrasts showed that negative outcomes (failing to win a reward and failing to avoid a loss) produced robust activity in the AI as well as in temporal and temporo-parietal regions. Subcortically, a post hoc ROI-level analysis showed that the anticipation of rewards produced more activation than did the anticipation of losses, including robust ventromedial striatal activity (Cohen's  $d$  in the ventromedial striatum was significantly different between the two contrasts,  $P < 10^{-4}$ ), while the putamen showed an opposite pattern for feedback with more activation when avoiding a loss than when winning a reward (Cohen's  $d$  in the putamen was significantly different,  $P < 0.0003$ ).

We also calculated the absolute maximum Pearson's correlation coefficient for cortical and subcortical activation measures for a single voxel and vertex per contrast and the variables age, puberty, education and scanner site. Overall, the vertex/voxelwise univariate analyses did not explain more than 1% of the variance associated with task activation (see Supplementary Tables 1 and 2 and Supplementary Notes 1 and 2 for more details). We also assessed the relationship between cortical thickness and functional brain activation in activated cortical regions for each fMRI task and found that cortical thickness did not explain more than 0.5% of the variance associated with BOLD activation in one single activated region (see Supplementary Fig. 1 and Supplementary Note 3 for more

details). In addition, we computed the correlation of BOLD activation across the three fMRI tasks and found very small associations among them (see Supplementary Fig. 2 and Supplementary Note 4 for more details). Finally, to determine if FD and the number of censored frames contaminate the activation estimates of each task, we computed the Pearson correlation coefficient between the Cohen's  $d$  maps as produced with our original set of covariates and Cohen's  $d$  maps computed when d.f. and FD, calculated per participant, were added as covariates. Activation maps were highly correlated after adding either d.f. or FD (see Supplementary Table 3, Supplementary Fig. 3 and Supplementary Note 5 for more details).

**Between-group task spatial reproducibility.** Cortical and subcortical Cohen's  $d$  correlation coefficients are shown for each task and contrast in Figs. 3e, 4e, 5c and 6c as a function of sample size. In addition, an HTML dynamic tool to display the correlation coefficients as a function of sample size is available for download in Supplementary Data 2 with a usage demo provided in Supplementary Fig. 4.

The cognitive, working memory contrasts of the EN-back task showed the strongest between-group spatial reproducibility, requiring a sample size of  $n=18$  for cortical and  $n=56$  for subcortical maps on average to reach a correlation coefficient of



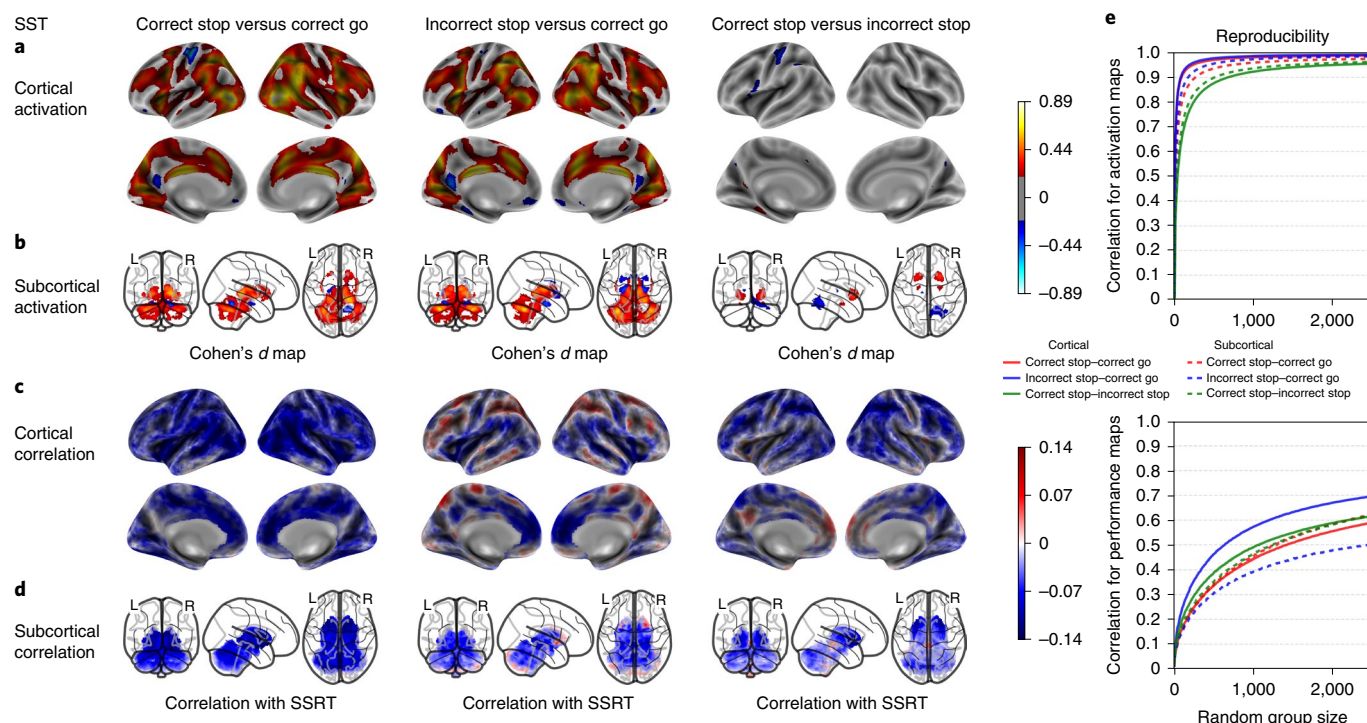


**Fig. 3 | SST activation maps, performance correlation maps and group-level spatial consistency at cortical and subcortical levels.** Activation maps (**a,b**), correlation maps (**c,d**) and reproducibility data (**e**) for the SST are shown. Cohen's *d* maps are thresholded at  $\geq 0.2$  in magnitude to only display small, medium and large effect sizes. No thresholding is applied to the correlation maps;  $N = 5,547$ .

0.8 or more across contrasts. Meanwhile, the emotional contrasts reached a maximum correlation coefficient of 0.75 with  $n = 2,500$ , except for cortical maps of the negative versus neutral faces contrast, requiring  $n = 1,285$  to reach a correlation coefficient of 0.8 or more (Figs. 4e and 5c). Group-level spatial reproducibility for the primary SST contrasts required a sample size of  $n = 32$  for cortical and  $n = 80$  for subcortical maps on average to reach a correlation coefficient of 0.8 or more across contrasts (Fig. 3e). Finally, the MID task required a sample size of  $n = 112$  for cortical and  $n = 143$  for subcortical maps on average to reach a correlation coefficient of 0.8 or more across the primary contrasts (Fig. 6c). Meanwhile, the secondary contrasts (anticipation of large versus small rewards and anticipation of large versus small losses) required a sample size of  $n = 775$  for cortical and  $n = 1,027$  on average for subcortical maps to reach a correlation coefficient of 0.8 or more (Fig. 6c).

**Individual differences.** Cortical and subcortical performance correlation maps of SST and EN-back contrasts are shown in Figs. 3c,d and 4c,d. In addition, static and 3D dynamic views of correlation coefficient maps are available online at the following address (download required to display the interactive maps): [https://drive.google.com/drive/folders/1VPnY8SS68JYis-AI-mt8\\_BJqc4r6GD5D](https://drive.google.com/drive/folders/1VPnY8SS68JYis-AI-mt8_BJqc4r6GD5D).

The correlation analyses between the SST beta weights and SSRT revealed that activation in individual vertices/voxels explained up to 2% of the individual performance differences in response inhibition. Whereas correlations were largely negative for the correct Stop contrast (faster SSRT accompanied by greater stop-related activation), a more varied pattern of positive and negative correlations was observed for the incorrect Stop contrast.

The performance correlation maps of the EN-back task largely recapitulated the task activation maps insofar as the correlations tended to be the largest where task activation was strongest. Activation in individual vertices/voxels explained up to 2.2% of

individual performance differences in working memory as measured by the EN-back  $D'$  accuracy metric.

In addition, we assessed performance correlation between the EN-back task and SST and found significant negative correlations, albeit with small coefficients of determination, between SSRT and  $D'$  for 0-back and 2-back tasks (see Supplementary Fig. 2 and Supplementary Note 4 for more details).

Finally, the spatial reproducibility of these brain performance correlation maps is shown in Figs. 3e and 4e. The reproducibility of these maps is notably smaller than the group activation maps, with up to 2,500 participants being insufficient in most cases to reach an asymptote of 0.8.

## Discussion

In this work, we reported fMRI activation patterns for SST, EN-back and MID tasks from the baseline assessment of the ABCD Study cohort. Further, we reported both the group-level spatial reproducibility of activation patterns as a function of sample size and the sensitivity of the activation maps to individual differences in behavioral task performance.

Overall, the task activation patterns observed in this study are consistent with the extant literature on adolescents and adults. The SST activation patterns replicate previous task fMRI SST data and meta-analyses in adults, adolescents and children insofar as the SST robustly activated regions known to play an important role in inhibitory control, such as the insula, superior/middle/inferior frontal gyrus, dACC/SMA, dlPFC, PPC, thalamus and basal ganglia (Rae et al.<sup>37</sup>,  $N = 331$ ; Hung et al.<sup>38</sup>,  $N = 1,447$ ; Swick et al.<sup>39</sup>,  $N = 440$ ). The correct and incorrect Stop maps were largely similar, likely indicating that the response inhibition circuitry is engaged even when the attempt to inhibit fails, which previous EEG data link to motor inhibition circuitry being activated, albeit too slowly, on commission errors<sup>40</sup>. The incorrect Stop maps do show greater activations than correct Stops in the left postcentral somato-sensorimotor

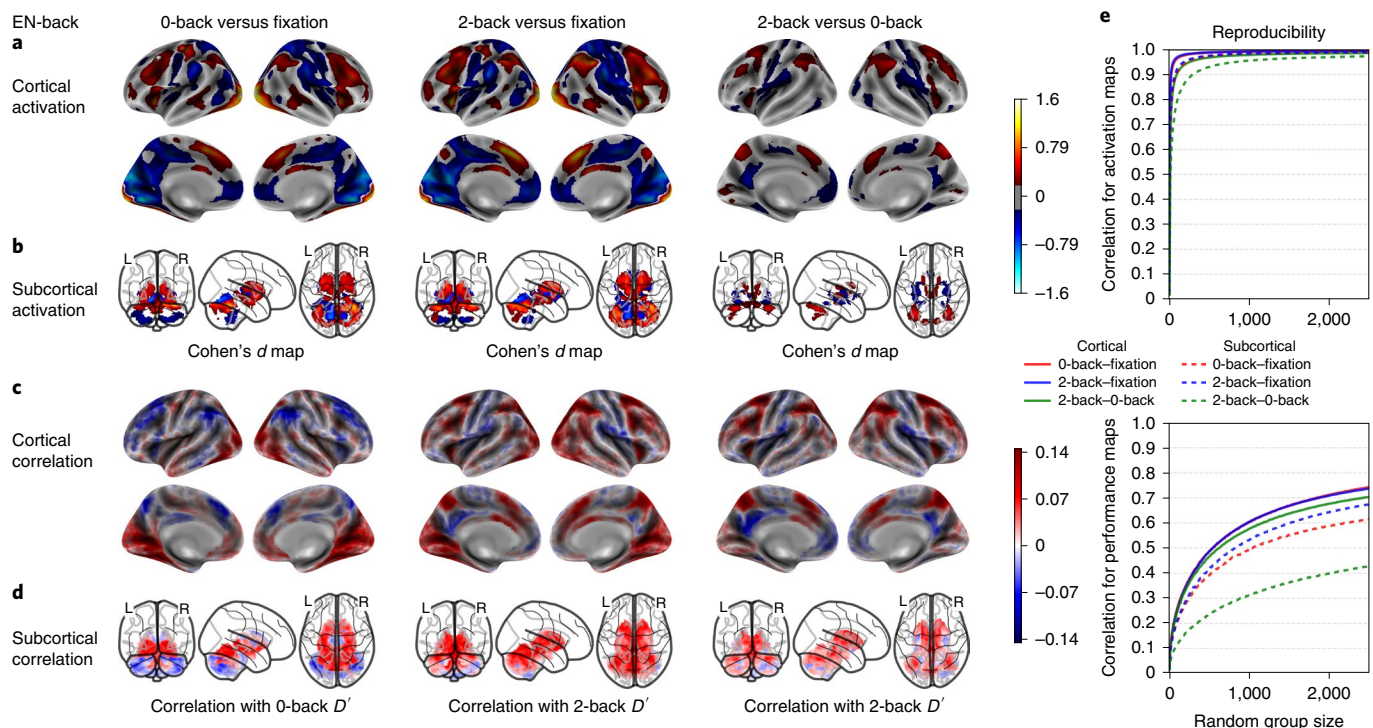


**Fig. 4 | EN-back task working memory activation maps, performance correlation maps and group-level spatial consistency at cortical and subcortical levels.** Working memory activation maps (**a,b**), correlation maps (**c,d**) and reproducibility data (**e**) for the EN-back task are shown. Cohen's *d* maps are thresholded at  $\geq 0.2$  in magnitude to only display small, medium and large effect sizes. No thresholding is applied to the correlation maps;  $N = 6,009$ .

gyrus, the AI and the dACC (mean Cohen's *d* significantly different at  $P < 0.001$ ), reflecting amplified right-handed motor and salience network activations when committing a commission error.

The regions activated by the 0-back versus fixation, 2-back versus fixation and 2-back versus 0-back conditions of the EN-back task included the dlPFC, PPC, SMA and AI. This activation pattern has been consistently observed across different N-back stimulus types and contrasts<sup>41</sup> as well as in an analysis, using the largest sample to date ( $N = 1,064$ ), of the EN-back task in the HCP<sup>18,36</sup>. The activation patterns are consistent with other tasks of working memory and executive functioning<sup>42</sup> and may constitute a unified cognitive control network<sup>43</sup>. Additionally, consistent with the deactivations we report, the EN-back task has been shown to reliably deactivate the DMN<sup>18,44</sup> relative to both resting and active baselines. This task was also shown to provide a useful probe of the intrinsic anticorrelation that has been proposed between cognitive control and DMN regions<sup>45</sup>. In line with our findings, a recent paper investigating the associations between working memory, cognitive abilities and fMRI activation in data from over 4,000 9- to 10-year-old participants enrolled in the ABCD Study<sup>16</sup> demonstrated that working memory function was significantly related to 2-back versus 0-back (that is, high versus low memory load) activation in regions of the frontal and parietal cortex, including the bilateral intraparietal sulci, dorsal premotor cortex/frontal eye fields, dlPFC, AI and dACC extending into the pre-SMA and precuneus. The results also revealed that working memory was not significantly associated with emotion-related activation during the EN-back task, inhibitory control-related activation during the SST or reward-related activation during the MID task. The faces versus places contrast yielded stimulus-specific activation in the amygdala, hippocampus and precuneus and in different regions of the visual cortex, including the FFA and OFA, consistent with evidence linking face viewing to the FFA and OFA<sup>22,26</sup> and place processing to the precuneus and

hippocampus<sup>46,47</sup>. The contrasts identifying differential responses to emotional faces, when compared with neutral faces, showed smaller Cohen's *d* effect sizes but have specific value by assaying social/emotional and memory processes (for example, heightened amygdalar response to negative faces) secondary to the primary focus on working memory.

The regions activated during reward anticipation in the MID task included the striatum, dACC, AI and parietal and occipital gyri, which is consistent with large studies ( $N > 830$ ) in children and adults, providing evidence that these regions are robustly associated with the reward anticipation condition of the MID task<sup>27,28,48</sup>. Similarly, the feedback contrasts showing activations in the PCC, vmPFC and VS are also consistent with this literature. However, in the large study by Cao et al.<sup>28</sup> using the IMAGEN dataset, only the vmPFC was activated by reward outcomes. When Silverman et al.<sup>27</sup> directly contrasted positive and negative valence events, they found positive events to be associated with greater activation in the VS, PCC, subcallosal gyrus and lateral occipital cortex. However, that study did not distinguish between anticipation and outcome phases. Subcortically, the present results showed higher activation in the ventromedial striatum for reward anticipation than for loss anticipation. In addition, there was higher activation when avoiding a loss (negative reinforcement) than when winning a reward in the ventrolateral striatum. These distinct reinforcement-related effects are consistent with a recent activation likelihood estimation meta-analysis of the MID task in 1,271 adults across 50 studies, which reported greater activation during reward anticipation than for reward outcome in the VS, insula and SMA; this meta-analysis also found greater activation for reward outcome than for reward anticipation in the vmPFC and PCC<sup>29</sup>. Comparing activation during the anticipation phase for large and small rewards, we observe a noticeable gradation in response, with a markedly lower activation across subcortical regions and the dorsomedial prefrontal, cingulate



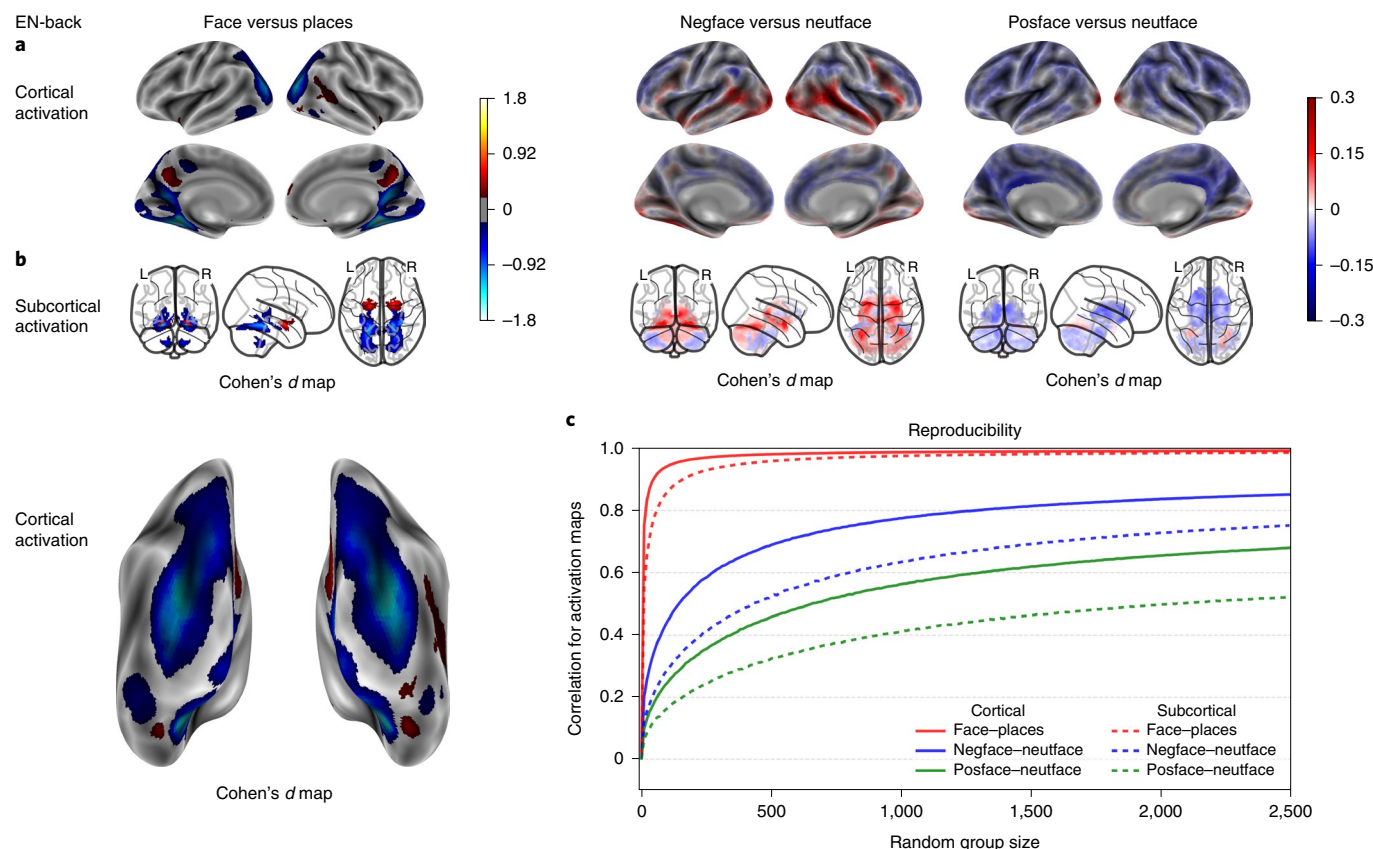


**Fig. 5 | EN-back task emotional activation maps, performance correlation maps and group-level spatial consistency at cortical and subcortical levels.** Emotional activation maps (**a,b**) and reproducibility data (**c**) for the EN-back task are shown. Cohen's *d* maps are thresholded at  $\geq 0.2$  in magnitude to only display small, medium and large effect sizes. No thresholding is applied to the correlation maps;  $N = 6,009$ ; negface, negative face; neutface, neutral face; posface, positive face.

and right inferior frontal cortex when anticipating smaller rewards. By contrast, we observe much less of a gradation in response during anticipation of loss. Although broader activation in the subcortex and right inferior frontal cortex during anticipation of a large (as opposed to small) loss is apparent, the gradation is less pronounced than for reward anticipation. These observations are consistent with a more general aversion to loss in contrast to a more value-dependent neural response in anticipation of reward.

**Group-level task spatial reproducibility.** The group-level spatial reproducibility plots demonstrated that group activation patterns for the primary contrasts of interest tend to be highly consistent across individuals for the SST, EN-back and MID tasks, highlighting the robust processes of interest involved in response inhibition, working memory and reward processing. The highest spatial reproducibility was observed in the EN-back task, particularly in working memory and faces versus places contrasts; this may reflect both the robustness of the cognitive processes it engages as well as task design features. Specifically, the EN-back task uses a block design, as opposed to the event-related designs of the SST and MID tasks, and does not require as fine-tuned a decomposition of the time series data such as that required, for example, by the more numerous regressors (that is, more conditions) of the MID task. Moreover, another factor influencing reproducibility is the number of trials per condition for any given participant, which is lower for the MID and emotional EN-back contrasts where lower spatial reproducibility coefficients are observed.

It is important to note that these analyses describe the spatial reproducibility of task fMRI with a focus on group-level data in

which we varied sample size. Thus, these results speak to the ability of tasks to generate the same activation patterns across separate groups of participants. They should not be interpreted as findings of test-retest reliability, which concerns whether individual differences in task activation are similar across different scanning sessions. Test-retest reliability is also an essential task design feature for a longitudinal study<sup>49</sup>. It cannot be assessed with just the single ABCD baseline assessment, and the subsequent biennial assessments introduce potential confounding data associated with developmental changes and perhaps even practice effects. However, this is a matter that can potentially be addressed with subsequent data releases. For example, there is variation in both the ages at which the baseline assessments were obtained (from 9 to 10) and variation in the intervals between the baseline and second assessments (scheduled for 2 years, but this can vary between 1 and 3 years), which, combined, may make it possible to estimate age and practice effects separately and consequently assess task test-retest reliability.

The present paper's group reproducibility findings may help inform the neuroscientific community on which tasks/contrasts from the ABCD dataset provide the most consistent maps for mean group statistics, which can, in turn, inform investigations comparing groups hypothesized to show activation differences.

**Task sensitivity to individual differences in performance.** The ranges in task performance and in ROI-level activation shown in Fig. 2 suggest that the tasks are suitable for exploring interindividual differences. The SST performance analyses showed that brain activations when successfully inhibiting were inversely correlated with SSRT; but, these vertex/voxelwise relationships were modest,



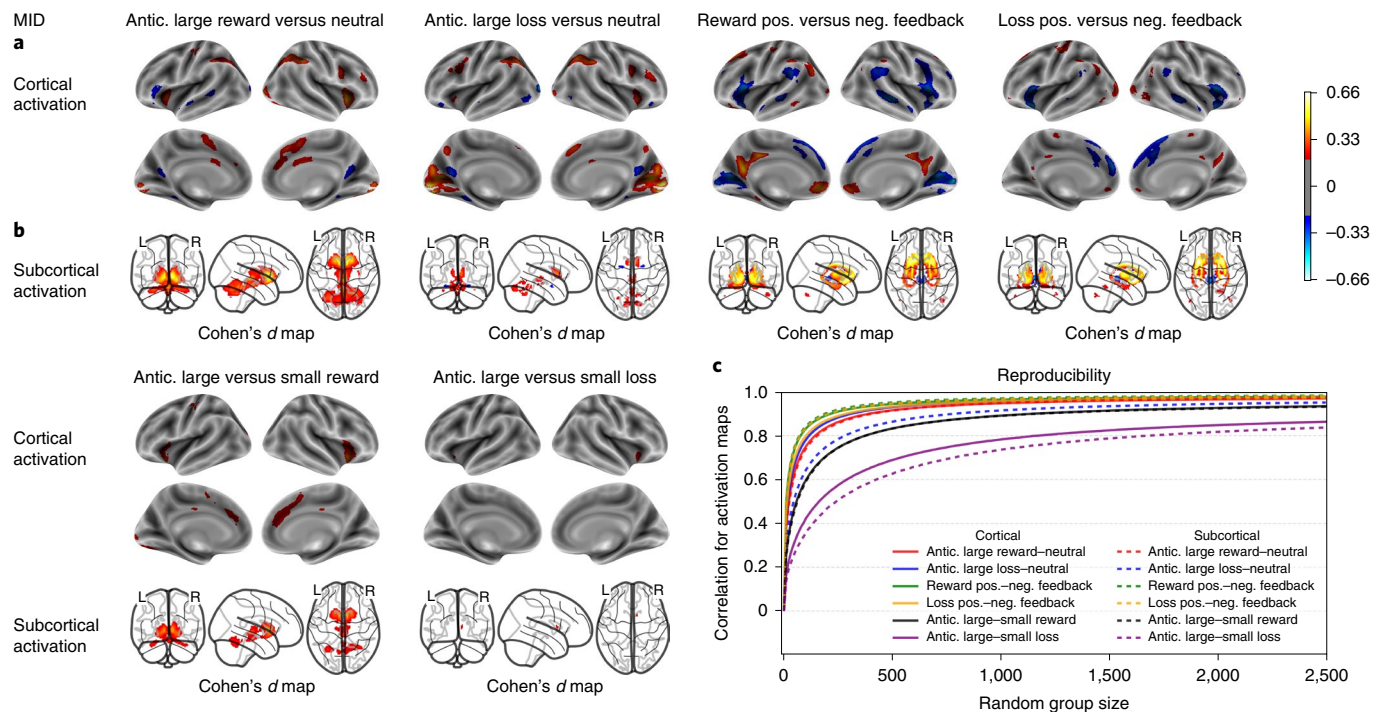


**Fig. 6 | MID task activation maps and group-level spatial consistency at cortical and subcortical levels.** Activation maps (a,b) and reproducibility data (c) for the MID task are shown. Cohen's *d* maps are thresholded at  $\geq 0.2$  in magnitude to only display small, medium and large effect sizes;  $N = 6,657$ ; Antic, anticipation of; pos, positive; neg, negative.

explaining a maximum of 2% ( $r = -0.14$ ) (lateral thalamic voxels) of the individual behavioral performance differences. It is noteworthy that more varied correlation patterns were observed for activity during incorrect Stops, with better inhibitors (that is, faster SSRT) showing greater activation in parts of the insula and the dlPFC. The areas showing these positive correlations with SSRT were those that likely reflect error-related processes (that is, more activation for incorrect Stops than correct Stops), suggesting a greater interoceptive and cognitive control response to errors in better inhibitors. Boehler et al.<sup>50</sup> previously reported the left AI to be the sole region showing a strong relationship between brain activity during stopping and SSRT ( $r = -0.69$  and  $-0.58$  depending on how SSRT was measured), albeit with a sample size of just 15 participants. In the EN-back task, performance analyses showed that brain activations were positively correlated with  $D'$  measures, explaining a maximum of 2.2% ( $r = 0.15$ ) of the individual behavioral performance differences (the strongest associations were observed in medial thalamic voxels).

The relatively small correlations between brain activation and performance on these two cognitive tasks highlight a fundamental challenge that motivates the ABCD Study. Namely, the size and scope of the ABCD Study provides an opportunity for a deep exploration of the mechanisms linking brain function to individual differences in numerous phenotypic measures and in individual developmental trajectories. Future research avenues include expanding beyond vertex/voxelwise associations to incorporate multivariate approaches and including other brain metrics, such as task connectivity, intrinsic connectivity, brain structure and anatomical connectivity. Improved assessments of behavior (for example, computational modeling of task performance) and brain (for example, incorporating individual differences in brain shape and function localization) may improve our ability to detect brain-behavior associations. Distal factors, such as genetics or in utero exposures, and current factors, such as exercise, sleep, education and other intellectual pursuits, may all contribute to the magnitude and patterns of brain-behavior associations. Consequently, incorporating

heterogeneity across participants (for example, biotyping) and exploiting the longitudinal aspects of the study wherein within-participant changes in behavior can be associated with within-participant neurodevelopmental changes may prove especially sensitive approaches for linking brain to behavior.

The large sample size of the ABCD Study enables researchers to move beyond group-level phenomena toward understanding interindividual differences and will, as the children age and repeat assessments are taken, elucidate intraindividual differences in brain function. Obtaining sensitive measurements of brain function will enable researchers to track changes in function reliably through development, assess how brain function co-develops with brain structure and identify what factors (genetic, environmental) affect brain development. Importantly, robust and reliable measures at the preadolescent stage will enable researchers to assess if future outcomes of interest (for example, mental health problems, substance use, academic excellence and resilience) can be predicted by baseline brain function, thereby informing etiological mechanisms. In addition, through the parallel assessment of behavior and any lagged changes that might be observed in relationship to brain function, researchers can identify plausible causal influences of those behaviors on brain development and vice versa.

The present results demonstrate robust fMRI activation patterns in tasks that engage inhibitory control, working memory and reward processing. They establish a well-characterized baseline from which to follow the children in the ABCD Study throughout adolescent development. Overall, the task activation patterns observed in this report are consistent with prior studies and underscore the value of the ABCD Study as a scientific resource for tracking changes in brain function during adolescence and into early adulthood. In addition to enabling cross-sectional analyses of interindividual and group differences, these activation patterns offer the potential for examining baseline predictors of future development and behavior and for quantifying changes in brain function that may arise from the numerous influences expected to affect development and behavior.

## Online content

Any methods, additional references, Nature Research reporting summaries, source data, extended data, supplementary information, acknowledgements, peer review information; details of author contributions and competing interests; and statements of data and code availability are available at <https://doi.org/10.1038/s41593-021-00867-9>.

Received: 31 December 2019; Accepted: 30 April 2021;

Published online: 07 June 2021

## References

- Membride, H. Mental health: early intervention and prevention in children and young people. *Br. J. Nurs.* **25**, 552–557 (2016).
- Verbruggen, F. et al. A consensus guide to capturing the ability to inhibit actions and impulsive behaviors in the stop-signal task. *eLife* **8**, e46323 (2019).
- Zhang, R., Geng, X. & Lee, T. M. C. Large-scale functional neural network correlates of response inhibition: an fMRI meta-analysis. *Brain Struct. Funct.* **222**, 3973–3990 (2017).
- Dwyer, D. B. et al. Large-scale brain network dynamics supporting adolescent cognitive control. *J. Neurosci.* **34**, 14096–14107 (2014).
- Luna, B., Marek, S., Larsen, B., Tervo-Clemmens, B. & Chahal, R. An integrative model of the maturation of cognitive control. *Annu. Rev. Neurosci.* **38**, 151–170 (2015).
- Ferdinand, N. K., & Kray, J. Developmental changes in performance monitoring: how electrophysiological data can enhance our understanding of error and feedback processing in childhood and adolescence. *Behav. Brain Res.* **263**, 122–132 (2014).
- Segalowitz, S. J., Santoso, D. L. & Jetha, M. K. Electrophysiological changes during adolescence: a review. *Brain Cogn.* **72**, 86–100 (2010).
- Alahyane, N., Brien, D. C., Coe, B. C., Stroman, P. W. & Munoz, D. P. Developmental improvements in voluntary control of behavior: effect of preparation in the fronto-parietal network? *Neuroimage* **98**, 103–117 (2014).
- Ordaz, S. J., Foran, W., Velanova, K. & Luna, B. Longitudinal growth curves of brain function underlying inhibitory control through adolescence. *J. Neurosci.* **33**, 18109–18124 (2013).
- Yaple, Z. A., Stevens, W. D. & Arsalidou, M. Meta-analyses of the n-back working memory task: fMRI evidence of age-related changes in prefrontal cortex involvement across the adult lifespan. *Neuroimage* **196**, 16–31 (2019).
- Rottschy, C. et al. Modelling neural correlates of working memory: a coordinate-based meta-analysis. *Neuroimage* **60**, 830–846 (2012).
- Yaple, Z. & Arsalidou, M. N-back working memory task: meta-analysis of normative fMRI studies with children. *Child Dev.* **89**, 2010–2022 (2018).
- Satterthwaite, T. D. et al. Functional maturation of the executive system during adolescence. *J. Neurosci.* **33**, 16249–16261 (2013).
- Thomason, M. E. et al. Development of spatial and verbal working memory capacity in the human brain. *J. Cogn. Neurosci.* **21**, 316–332 (2009).
- O'Hare, E. D., Lu, L. H., Houston, S. M., Bookheimer, S. Y. & Sowell, E. R. Neurodevelopmental changes in verbal working memory load-dependency: an fMRI investigation. *Neuroimage* **42**, 1678–1685 (2008).
- Rosenberg, M. D. et al. Behavioral and neural signatures of working memory in childhood. *J. Neurosci.* **40**, 5090–5104 (2020).
- Schweizer, S. et al. The impact of affective information on working memory: a pair of meta-analytic reviews of behavioral and neuroimaging evidence. *Psychol. Bull.* **145**, 566–609 (2019).
- Barch, D. M. et al. Function in the human connectome: task-fMRI and individual differences in behavior. *Neuroimage* **80**, 169–189 (2013).
- Gauthier, I. et al. The fusiform 'face area' is part of a network that processes faces at the individual level. *J. Cogn. Neurosci.* **12**, 495–504 (2000).
- Fuhrmann, D. et al. Perception and recognition of faces in adolescence. *Sci. Rep.* **6**, 33497 (2016).
- Cohen Kadosh, K. Differing processing abilities for specific face properties in mid-childhood and adulthood. *Front. Psychol.* **2**, 400 (2012).
- Scherf, K. S., Behrmann, M. & Dahl, R. E. Facing changes and changing faces in adolescence: a new model for investigating adolescent-specific interactions between pubertal, brain and behavioral development. *Dev. Cogn. Neurosci.* **2**, 199–219 (2012).
- Tahmasebi, A. M. et al. Creating probabilistic maps of the face network in the adolescent brain: a multicentre functional MRI study. *Hum. Brain Mapp.* **33**, 938–957 (2012).
- Kadosh, K. C. What can emerging cortical face networks tell us about mature brain organisation? *Dev. Cogn. Neurosci.* **1**, 246–255 (2011).
- Cohen Kadosh, K., Johnson, M. H., Henson, R. N. A., Dick, F. & Blakemore, S.-J. Differential face-network adaptation in children, adolescents and adults. *Neuroimage* **69**, 11–20 (2013).
- Scherf, K. S., Behrmann, M., Humphreys, K. & Luna, B. Visual category-selectivity for faces, places and objects emerges along different developmental trajectories. *Dev. Sci.* **10**, F15–F30 (2007).
- Silverman, M. H., Jedd, K. & Luciana, M. Neural networks involved in adolescent reward processing: an activation likelihood estimation meta-analysis of functional neuroimaging studies. *Neuroimage* **122**, 427–439 (2015).
- Cao, Z. et al. Mapping adolescent reward anticipation, receipt, and prediction error during the monetary incentive delay task. *Hum. Brain Mapp.* **40**, 262–283 (2019).
- Oldham, S. et al. The anticipation and outcome phases of reward and loss processing: a neuroimaging meta-analysis of the monetary incentive delay task. *Hum. Brain Mapp.* **39**, 3398–3418 (2018).
- Falk, E. B. et al. What is a representative brain? Neuroscience meets population science. *Proc. Natl Acad. Sci. USA* **110**, 17615–17622 (2013).
- Baker, M. 1,500 scientists lift the lid on reproducibility. *Nature* **533**, 452–454 (2016).
- Song, X., Panych, L. P., Chou, Y.-H. & Chen, N.-K. A study of long-term fMRI reproducibility using data-driven analysis methods. *Int. J. Imaging Syst. Technol.* **24**, 339–349 (2014).
- Thirion, B. et al. Analysis of a large fMRI cohort: statistical and methodological issues for group analyses. *Neuroimage* **35**, 105–120 (2007).
- Turner, B. O., Paul, E. J., Miller, M. B. & Barbey, A. K. Small sample sizes reduce the replicability of task-based fMRI studies. *Commun. Biol.* **1**, 1–10 (2018).
- Van Essen, D. C. et al. The WU-Minn Human Connectome Project: an overview. *Neuroimage* **80**, 62–79 (2013).
- Owens, M. M., Duda, B., Sweet, L. H. & MacKillop, J. Distinct functional and structural neural underpinnings of working memory. *Neuroimage* **174**, 463–471 (2018).
- Rae, C. L., Hughes, L. E., Weaver, C., Anderson, M. C. & Rowe, J. B. Selection and stopping in voluntary action: a meta-analysis and combined fMRI study. *Neuroimage* **86**, 381–391 (2014).
- Hung, Y., Gaillard, S. L., Yarmak, P. & Arsalidou, M. Dissociations of cognitive inhibition, response inhibition, and emotional interference: voxelwise ALE meta-analyses of fMRI studies. *Hum. Brain Mapp.* **39**, 4065–4082 (2018).
- Swick, D., Ashley, V. & Turken, U. Are the neural correlates of stopping and not going identical? Quantitative meta-analysis of two response inhibition tasks. *Neuroimage* **56**, 1655–1665 (2011).
- Garavan, H., Ross, T. J., Murphy, K., Roche, R. A. P. & Stein, E. A. Dissociable executive functions in the dynamic control of behavior: inhibition, error detection, and correction. *Neuroimage* **17**, 1820–1829 (2002).
- Owen, A. M., McMillan, K. M., Laird, A. R. & Bullmore, E. N-back working memory paradigm: a meta-analysis of normative functional neuroimaging studies. *Hum. Brain Mapp.* **25**, 46–59 (2005).
- Wager, T. D. & Smith, E. E. Neuroimaging studies of working memory: a meta-analysis. *Cogn. Affect. Behav. Neurosci.* **3**, 255–274 (2003).
- Niendam, T. A. et al. Meta-analytic evidence for a superordinate cognitive control network subserving diverse executive functions. *Cogn. Affect. Behav. Neurosci.* **12**, 241–268 (2012).
- Buckner, R. L., Andrews-Hanna, J. R. & Schacter, D. L. The brain's default network: anatomy, function, and relevance to disease. *Ann. N. Y. Acad. Sci.* **1124**, 1–38 (2008).
- Fox, M. D. et al. The human brain is intrinsically organized into dynamic, anticorrelated functional networks. *Proc. Natl Acad. Sci. USA* **102**, 9673–9678 (2005).
- Baird, A. A. et al. Functional magnetic resonance imaging of facial affect recognition in children and adolescents. *J. Am. Acad. Child Adolesc. Psychiatry* **38**, 195–199 (1999).
- Hare, T. A. et al. Biological substrates of emotional reactivity and regulation in adolescence during an emotional go-nogo task. *Biol. Psychiatry* **63**, 927–934 (2008).
- Heitzeg, M. M. et al. Effect of GABRA2 genotype on development of incentive-motivation circuitry in a sample enriched for alcoholism risk. *Neuropsychopharmacology* **39**, 3077–3086 (2014).
- Elliott, M. L. et al. What is the test-retest reliability of common task-functional MRI measures? New empirical evidence and a meta-analysis. *Psychol. Sci.* **31**, 792–806 (2020).
- Boehler, C. N., Appelbaum, L. G., Krebs, R. M., Hopf, J.-M. & Woldorff, M. G. The influence of different Stop-signal response time estimation procedures on behavior-behavior and brain-behavior correlations. *Behav. Brain Res.* **229**, 123–130 (2012).
- Casey, B. J. et al. The Adolescent Brain Cognitive Development (ABCD) study: imaging acquisition across 21 sites. *Dev. Cogn. Neurosci.* **32**, 43–54 (2018).

**Publisher's note** Springer Nature remains neutral with regard to jurisdictional claims in published maps and institutional affiliations.

© The Author(s), under exclusive licence to Springer Nature America, Inc. 2021

B. Chaarani<sup>1</sup>✉, S. Hahn<sup>1</sup>, N. Allgaier<sup>1</sup>, S. Adise<sup>1</sup>, M. M. Owens<sup>1</sup>, A. C. Juliano<sup>1</sup>, D. K. Yuan<sup>1</sup>, H. Loso<sup>1</sup>, A. Ivanciu<sup>1</sup>, M. D. Albaugh<sup>1</sup>, J. Dumas<sup>1</sup>, S. Mackey<sup>1</sup>, J. Laurent<sup>1</sup>, M. Ivanova<sup>1</sup>, D. J. Hagler<sup>2</sup>, M. D. Cornejo<sup>3</sup>, S. Hatton<sup>2</sup>, A. Agrawal<sup>4</sup>, L. Aguinaldo<sup>2</sup>, L. Ahonen<sup>5</sup>, W. Aklin<sup>6</sup>, A. P. Anokhin<sup>4</sup>, J. Arroyo<sup>7</sup>, S. Avenevoli<sup>8</sup>, D. Babcock<sup>9</sup>, K. Bagot<sup>10</sup>, F. C. Baker<sup>11</sup>, M. T. Banich<sup>12</sup>, D. M. Barch<sup>4</sup>, H. Bartsch<sup>13</sup>, A. Baskin-Sommers<sup>14</sup>, J. M. Bjork<sup>15</sup>, D. Blachman-Demner<sup>16</sup>, M. Bloch<sup>17</sup>, R. Bogdan<sup>4</sup>, S. Y. Bookheimer<sup>18</sup>, F. Breslin<sup>19</sup>, S. Brown<sup>2</sup>, F. J. Calabro<sup>5</sup>, V. Calhoun<sup>12,20</sup>, B. J. Casey<sup>14</sup>, L. Chang<sup>21</sup>, D. B. Clark<sup>5</sup>, C. Cloak<sup>21</sup>, R. T. Constable<sup>14</sup>, K. Constable<sup>6</sup>, R. Corley<sup>12</sup>, L. B. Cottler<sup>22</sup>, S. Coxe<sup>23</sup>, R. K. Dagher<sup>24</sup>, A. M. Dale<sup>2</sup>, M. Dapretto<sup>18</sup>, R. Delcarmen-Wiggins<sup>25</sup>, A. S. Dick<sup>23</sup>, E. K. Do<sup>15</sup>, N. U. F. Dosenbach<sup>4</sup>, G. J. Dowling<sup>6</sup>, S. Edwards<sup>21</sup>, T. M. Ernst<sup>21</sup>, D. A. Fair<sup>26</sup>, C. C. Fan<sup>4</sup>, E. Feczko<sup>26</sup>, S. W. Feldstein-Ewing<sup>26</sup>, P. Florsheim<sup>27</sup>, J. J. Foxe<sup>28</sup>, E. G. Freedman<sup>28</sup>, N. P. Friedman<sup>12</sup>, S. Friedman-Hill<sup>8</sup>, B. F. Fuemmeler<sup>15</sup>, A. Galvan<sup>18</sup>, D. G. Gee<sup>14</sup>, J. Giedd<sup>2</sup>, M. Glantz<sup>6</sup>, P. Glaser<sup>4</sup>, J. Godino<sup>2</sup>, M. Gonzalez<sup>29</sup>, R. Gonzalez<sup>23</sup>, S. Grant<sup>6</sup>, K. M. Gray<sup>30</sup>, F. Haist<sup>2</sup>, M. P. Harms<sup>4</sup>, S. Hawes<sup>23</sup>, A. C. Heath<sup>2</sup>, S. Heeringa<sup>31</sup>, M. M. Heitzeg<sup>31</sup>, R. Hermosillo<sup>26</sup>, M. M. Herting<sup>32</sup>, J. M. Hettema<sup>15</sup>, J. K. Hewitt<sup>12</sup>, C. Heyser<sup>2</sup>, E. Hoffman<sup>6</sup>, K. Howlett<sup>6</sup>, R. S. Huber<sup>33</sup>, M. A. Huestis<sup>34</sup>, L. W. Hyde<sup>31</sup>, W. G. Iacono<sup>35</sup>, M. A. Infante<sup>2</sup>, O. Irfanoglu<sup>36</sup>, A. Isaiah<sup>21</sup>, S. Iyengar<sup>37</sup>, J. Jacobus<sup>2</sup>, R. James<sup>15</sup>, B. Jean-Francois<sup>24</sup>, T. Jernigan<sup>2</sup>, N. R. Karcher<sup>4</sup>, A. Kaufman<sup>17</sup>, B. Kelley<sup>38</sup>, B. Kit<sup>39</sup>, A. Ksinan<sup>15</sup>, J. Kuperman<sup>2</sup>, A. R. Laird<sup>23</sup>, C. Larson<sup>27</sup>, K. LeBlanc<sup>6</sup>, C. Lessov-Schlagger<sup>4</sup>, N. Lever<sup>21</sup>, D. A. Lewis<sup>5</sup>, K. Lisdahl<sup>27</sup>, A. R. Little<sup>6</sup>, M. Lopez<sup>6</sup>, M. Luciana<sup>35</sup>, B. Luna<sup>5</sup>, P. A. Madden<sup>4</sup>, H. H. Maes<sup>15</sup>, C. Makowski<sup>2</sup>, A. T. Marshall<sup>29</sup>, M. J. Mason<sup>40</sup>, J. Matochik<sup>7</sup>, B. D. McCandliss<sup>41</sup>, E. McGlade<sup>33</sup>, I. Montoya<sup>6</sup>, G. Morgan<sup>17</sup>, A. Morris<sup>42</sup>, C. Mulford<sup>6</sup>, P. Murray<sup>7</sup>, B. J. Nagel<sup>26</sup>, M. C. Neale<sup>15</sup>, G. Neigh<sup>15</sup>, A. Nencka<sup>43</sup>, A. Noronha<sup>7</sup>, S. J. Nixon<sup>22</sup>, C. E. Palmer<sup>2</sup>, V. Pariyadath<sup>6</sup>, M. P. Paulus<sup>19</sup>, W. E. Pelham<sup>23</sup>, D. Pfefferbaum<sup>11</sup>, C. Pierpaoli<sup>44</sup>, A. Prescott<sup>33</sup>, D. Prouty<sup>11</sup>, L. I. Puttler<sup>31</sup>, N. Rajapaske<sup>24</sup>, K. M. Rapuano<sup>14</sup>, G. Reeves<sup>21</sup>, P. F. Renshaw<sup>33</sup>, M. C. Riedel<sup>23</sup>, P. Rojas<sup>23</sup>, M. de la Rosa<sup>23</sup>, M. D. Rosenberg<sup>45</sup>, M. J. Ross<sup>46</sup>, M. Sanchez<sup>23</sup>, C. Schirda<sup>5</sup>, D. Schloesser<sup>16</sup>, J. Schulenberg<sup>31</sup>, K. J. Sher<sup>47</sup>, C. Sheth<sup>33</sup>, P. D. Shilling<sup>2</sup>, W. K. Simmons<sup>19</sup>, E. R. Sowell<sup>29</sup>, N. Speer<sup>12</sup>, M. Spittel<sup>16</sup>, L. M. Squeglia<sup>30</sup>, C. Sripada<sup>31</sup>, J. Steinberg<sup>15</sup>, C. Striley<sup>22</sup>, M. T. Sutherland<sup>23</sup>, J. Tanabe<sup>12</sup>, S. F. Tapert<sup>2</sup>, W. Thompson<sup>2</sup>, R. L. Tomko<sup>30</sup>, K. A. Uban<sup>48</sup>, S. Vrieze<sup>35</sup>, N. E. Wade<sup>2</sup>, R. Watts<sup>14</sup>, S. Weiss<sup>6</sup>, B. A. Wiens<sup>22</sup>, O. D. Williams<sup>23</sup>, A. Wilbur<sup>11</sup>, D. Wing<sup>2</sup>, D. Wolff-Hughes<sup>16</sup>, R. Yang<sup>2</sup>, D. A. Yurgelun-Todd<sup>33</sup>, R. A. Zucker<sup>31</sup>, A. Potter<sup>1</sup>, H. P. Garavan<sup>1</sup>✉ and the ABCD Consortium\*

<sup>1</sup>Department of Psychiatry, University of Vermont, Burlington, VT, USA. <sup>2</sup>University of California, San Diego, La Jolla, CA, USA. <sup>3</sup>Institute of Physics UC, Pontificia Universidad Catolica de Chile, Pontificia, Chile. <sup>4</sup>Department of Psychiatry, Washington University in Saint Louis, St. Louis, MO, USA. <sup>5</sup>University of Pittsburgh, Pittsburgh, PA, USA. <sup>6</sup>National Institute on Drug Abuse, Bethesda, MD, USA. <sup>7</sup>National Institute on Alcohol Abuse and Alcoholism, Bethesda, MD, USA. <sup>8</sup>National Institute of Mental Health, Bethesda, MD, USA. <sup>9</sup>National Institute of Neurological Disorders and Stroke, Bethesda, MD, USA. <sup>10</sup>Icahn School of Medicine at Mount Sinai, New York, NY, USA. <sup>11</sup>SRI International, Menlo Park, CA, USA. <sup>12</sup>University of Colorado, Boulder, CO, USA. <sup>13</sup>Haukeland University Hospital, Bergen, Norway. <sup>14</sup>Yale University, New Haven, CT, USA. <sup>15</sup>Virginia Commonwealth University, Richmond, VA, USA. <sup>16</sup>NIH Office of Behavioral and Social Sciences Research, Bethesda, MD, USA. <sup>17</sup>National Cancer Institute, Bethesda, MD, USA. <sup>18</sup>University of California, Los Angeles, CA, USA. <sup>19</sup>Laureate Institute for Brain Research, Tulsa, OK, USA. <sup>20</sup>Tri-institutional Center for Translational Research in Neuroimaging and Data Science, Georgia State University, Georgia Institute of Technology, Emory University, Atlanta, GA, USA. <sup>21</sup>University of Maryland School of Medicine, Baltimore, MD, USA. <sup>22</sup>University of Florida, Gainesville, FL, USA. <sup>23</sup>Florida International University, Miami, FL, USA. <sup>24</sup>National Institute on Minority Health and Health Disparities, Bethesda, MD, USA. <sup>25</sup>NIH Office of Research on Women's Health, Bethesda, MD, USA. <sup>26</sup>Oregon Health & Science University, Portland, OR, USA. <sup>27</sup>University of Wisconsin, Milwaukee, WI, USA. <sup>28</sup>University of Rochester, Rochester, NY, USA. <sup>29</sup>Children's Hospital Los Angeles, Los Angeles, CA, USA. <sup>30</sup>Medical University of South Carolina, Charleston, SC, USA. <sup>31</sup>University of Michigan, Ann Arbor, MI, USA. <sup>32</sup>University of Southern California, Los Angeles, CA, USA. <sup>33</sup>University of Utah, Salt Lake City, UT, USA. <sup>34</sup>Thomas Jefferson University, Philadelphia, PA, USA. <sup>35</sup>University of Minnesota, Minneapolis, MN, USA. <sup>36</sup>National Institute of Biomedical Imaging and Bioengineering, Bethesda, MD, USA. <sup>37</sup>National Endowment for the Arts, Washington DC, USA. <sup>38</sup>National Institute of Justice, Washington DC, USA. <sup>39</sup>National Heart, Lung, and Blood Institute, Bethesda, MD, USA. <sup>40</sup>University of Tennessee, Knoxville, TN, USA. <sup>41</sup>Stanford University, Stanford, CA, USA. <sup>42</sup>Oklahoma State University, Stillwater, OK, USA. <sup>43</sup>Medical College of Wisconsin, Milwaukee, WI, USA. <sup>44</sup>Eunice Kennedy Shriver National Institute of Child Health and Human Development, Bethesda, MD, USA. <sup>45</sup>University of Chicago, Chicago, IL, USA. <sup>46</sup>University of Colorado Anschutz Medical Campus, Aurora, CO, USA. <sup>47</sup>University of Missouri, Columbia, MO, USA. <sup>48</sup>University of California, Irvine, CA, USA. \*A list of authors and their affiliations appears at the end of the paper. ✉e-mail: [melmarsr@uvm.edu](mailto:melmarsr@uvm.edu); [hgaravan@uvm.edu](mailto:hgaravan@uvm.edu)



## Methods

**Sample.** The ABCD sample was largely recruited through public, private and charter elementary schools. ABCD adopted a population neuroscience approach to recruitment<sup>30,52</sup> by using epidemiologically informed procedures to ensure demographic variation in its sample that would mirror the variation in the US population of 9- and 10-year-olds<sup>53</sup>. A probability sampling of schools was conducted within the defined catchment areas of the study's nationally distributed set of 21 recruitment sites. All children in each sampled school were invited to participate following classroom-based presentations, distribution of study materials and telephone screening for eligibility. Exclusions included common MRI contraindications (such as cardiac pacemakers and defibrillators, internal pacing wires, cochlear and metallic implants and Swan–Ganz catheters), inability to understand or speak English fluently, uncorrected vision, hearing or sensorimotor impairments, a history of major neurological disorders, gestational age <28 weeks, birth weight <1,200 g, birth complications that resulted in hospitalization for more than 1 month, current diagnosis of schizophrenia, moderate or severe autism spectrum disorder, a history of traumatic brain injury or unwillingness to complete assessments. The ABCD sample also includes 2,105 monozygotic and dizygotic twins. Consent (parents) and assent (children) were obtained from all participants, and the ABCD Study was approved by the appropriate institutional review boards. Data collection and analyses were not performed blind to the conditions of the experiments. The ABCD Study's anonymized and curated data, including all assessment domains, are released annually to the research community. The ABCD Study is a single cohort, observational and longitudinal design that has no randomization of participants to groups. Information on how to access ABCD data through the NIMH Data Archive (NDA) is available on the ABCD Study data-sharing webpage [https://abcdstudy.org/scientists\\_data\\_sharing.html](https://abcdstudy.org/scientists_data_sharing.html). Further information on research design is available in the Reporting Summary linked to this article.

Inclusion criteria for the current study were predetermined by the ABCD DAIR<sup>51</sup>. In brief, participants were included if they had (1) two fMRI runs per task, (2) cortical vertex and subcortical voxel data available at the time of analysis, (3) hemispheric mean beta weights within 2 s.d. of the sample mean for each task, (4) at least 200 d.f. over the two scan runs, (5) a mean FD <0.9 mm for both runs, (6) met task-specific performance criteria (described in Behavioral task performance) and (7) complete information for covariates of interest (age, sex, scanner serial number, race and puberty<sup>54</sup>) and highest parent education (see Table 1 for details on datapoints that were excluded from analyses, the rationale and the number of participants remaining after each step of exclusions). This resulted in varying sample sizes and demographics among the fMRI tasks. No statistical methods were used to predetermine sample sizes, but our sample sizes exceed those reported in previous publications<sup>18,28,35</sup>. Given these large sample sizes, data distribution was assumed to be normal, although this was not formally tested (see Fig. 2 for details on data distributions).

Task fMRI data for 1,512 participants obtained on Philips scanners were also excluded from this paper due to incorrect post-processing. Corrected data will be available in the ABCD Data Release 3.0. An official statement providing more details is available on the ABCD Study website ([https://abcdstudy.org/scientists\\_data-sharing/](https://abcdstudy.org/scientists_data-sharing/)). An R script is available at <https://github.com/ABCD-STUDY/fMRI-cleanup> to remove Philips fMRI data from tabulated data. Table 2 presents the demographic composition of both samples who were included and who were excluded from the current study. Although the differences between these two samples are statistically significant, which is not surprising with over 10,000 participants in the analyses, the effect sizes were small (Cramer's  $V \leq 0.16$ ), and, most importantly, the fMRI samples showed considerable demographic diversity (and in this regard are very similar to the full sample). In addition, propensity weighting scores are available in the ABCD Data Analysis and Exploration Portal (DEAP) for researchers who wish to adjust sample estimates to population-level demographics.

**fMRI tasks.** The ABCD Study's fMRI behavioral tasks include the SST, EN-back task and MID task. These tasks were selected to probe inhibitory control, emotion processing and working memory and reward processing<sup>51</sup>. Participants practiced the three tasks before scanning to ensure that they understood the instructions and were familiar with the response collection device. While the fMRI tasks were always collected last as part of the fixed order of the scanning session, the order in which the fMRI tasks occurred was randomized across participants as well as the ordering of the event-related fMRI task's trials. There were 12 trial-order variations (pseudorandomized) of the SST and MID tasks. Siblings were given the same order of scans and trial-order version of the MID task and SST to minimize within-family variability. For further details, see Casey et al.<sup>51</sup>. The ABCD imaging protocol was designed to extend the benefits of high temporal and spatial resolution of imaging protocols of the HCP<sup>55</sup> with the multiple scanner systems of participating sites<sup>56</sup>.

**SST.** The SST<sup>57</sup> presented leftward and rightward facing arrows in serial order ('Go' stimuli). Participants indicated the direction of the arrows using a two-button response box (left and right buttons). Participants were instructed to respond as

quickly and accurately as possible, but were told not to respond on trials in which a left or right arrow was followed by an arrow pointing upward (the 'Stop' signal).

The SST had an event-related design with two runs. Each had 180 trials, of which 30 were 'Stop' trials, yielding a total of 60 'Stop' trials and 300 'Go' trials. Each trial lasted 1 s. The time between the 'Go' and 'Stop' signals (SSD) varied dynamically based on a participant's success on the prior trial so as to achieve a 50% success rate (starting at 50 ms, the SSD increased by 50 ms if the participant successfully stopped on the previous trial and decreased by 50 ms if they responded; Fig. 1a).

**EN-back task.** The EN-back task was a modified version of a traditional N-back task<sup>18,58</sup> using a block design that added elements of facial and emotional processing. This task was designed so that through fMRI contrast subtraction it would be possible to investigate working memory, facial recognition and emotional processes independently or to investigate the interaction between working memory, faces and emotion. The current analysis focused on contrasts that isolated working memory and facial recognition/emotion; these contrasts were shown to be effective in eliciting neural responses consistent with standard working memory, facial recognition and emotion in adults in the task's original usage in the HCP<sup>18</sup>. Participants saw a series of stimuli and indicated whether each one was the same or different than the stimulus  $N$  items earlier (that is, 'N back'). The EN-back task had two conditions: a 2-back as the active condition and a 0-back as the baseline condition, which included similar visuomotor demands but lower working memory load. In the 0-back condition, participants indicated if each stimulus matched a single target presented at the beginning of the block, thereby obviating the need to maintain and update a two-item working memory load throughout the task. Responses on the 2-back and 0-back were input on a two-button keypad, with one button indicating the stimulus was a match and the other indicating no match (Fig. 1b).

The EN-back consisted of two runs, each containing eight blocks of trials and four 15-s periods containing just a fixation cross. Blocks contained ten trials lasting 2.5 s each and were preceded by a 2.5-s instruction screen indicating the condition for the upcoming block. Of the ten trials in each block, two were targets, two to three were non-target lures and the remainder were non-lures (that is, stimuli only presented once). There were 160 trials in total with 96 unique stimuli of 4 different stimulus types (24 unique stimuli per type). Three-quarters of the stimuli types were human faces, demonstrating happy, fearful or neutral facial expressions, with facial expression stimulus type held constant within each block. The faces used were all adult faces, which was considered ideal given previous research suggesting that children demonstrate similar but stronger neural responses to adult faces relative to child faces<sup>59,60</sup>. Faces were racially diverse and derived from two preexisting collections: the NimStim emotional stimulus set<sup>61</sup> and the racially diverse affective expressions (RADIATE) set of stimuli<sup>62</sup>. Additionally, images of places were used as a fourth stimulus type. The place stimuli were taken from prior visual perception studies<sup>63,64</sup>. For the working memory component, the main contrast was a block design analysis contrasting 2-back and 0-back (eight blocks each). Finally, a post-scan recognition memory test was performed<sup>18,51</sup> to measure memory processes associated with hippocampal functioning. The task included 48 old stimuli presented during the EN-back task and 48 new stimuli, with equal numbers of each stimulus type in the old and new stimulus sets (12 each of happy, fearful and neutral facial expressions as well as places in each set). Ninety-six pictures were presented during the recognition memory test. Participants were asked to rate each picture as either 'Old' or 'New'. Each picture was presented for 2 s followed immediately by a 1-s presentation of a fixation cross. The task assessed memory for stimuli presented during the EN-back and took approximately 5–10 min.

**MID task.** The MID task included both anticipation and receipt of reward and loss<sup>65,66</sup>. Participants attempted to win money or avoid losing money by quickly responding to cued stimuli using a response box in their dominant hand. This task is entirely focused on response time rather than response choice; hence, there was only one response option on this task. For 'win' trials, participants could win or 'not win' US\$5.00 or US\$0.20 depending on whether they responded in the time allotted. For 'lose' trials, they could either 'not lose' or lose the same amounts by responding within the time frame. In 'neutral' trials, participants completed the same action but with no money available to be won or lost (Fig. 1c).

The MID task had an event-related design. The specific sequence of each trial was as follows: participants saw a cue denoting the trial type (2 s), with win trials shown in a pink circle, lose trials shown in a yellow square and neutral trials shown in a blue triangle. Then, participants viewed a fixation cross of jittered duration (1.5–4 s), followed by a signal to respond, denoted by a black shape that corresponded to the trial type. The duration in which participants were able to respond (that is, duration of the response signal) varied between trials (0.15–0.5 s). The time allowed to respond at the beginning of the task was determined by the participant's performance during a practice session before scanning and, during scanning, was adjusted after every third incentivized trial based on the overall accuracy rate of the previous six trials to produce a 60% accuracy rate across the task. If the participant's accuracy fell below the target accuracy level, the duration of the target was lengthened. If the participant's



accuracy was above the target accuracy level, the target duration was shortened. Immediately after responding, participants received written feedback (for example, 'You won \$5'), which was presented for 2 s minus the duration of the response target. Each run consisted of 50 contiguous trials (10 per trial type) presented in pseudorandom order and lasted 5 min and 42 s. Participants were compensated based on their performance on the task (mean earnings, US\$20; maximum possible earnings, US\$60).

**fMRI acquisition and preprocessing.** High spatial and temporal resolution simultaneous multislice/multiband echo-planar imaging (EPI) task-based fMRI scans with fast integrated distortion correction were acquired to examine functional activity. For Siemens and GE 3 T scanners, the following scanning parameters were used: matrix of 90 × 90, 60 slices, field of view (FOV) = 216 × 216, echo time (TE)/repetition time (TR) (ms) = 800/30, flip angle = 52° and resolution (mm) = 2.4 × 2.4 × 2.4. The fMRI acquisitions (2.4 mm isotropic, TR = 800 ms) used multiband EPI with slice acceleration factor 6. The order of the three fMRI tasks was randomized across participants. The full details of the imaging acquisition protocol were previously described in Casey et al.<sup>51</sup>. The ABCD Data Analysis, Informatics and Resource Center (DAIRC) performed centralized initial quality control and processing of the fMRI data. All MRI assessments were reviewed by a neuroradiologist for incidental findings. Using a combination of automated and manual methods, the fMRI datasets were quality controlled for problems, such as acquisition protocol compliance, imaging artifacts, motion or file corruption. Processing steps subsequent to fMRI preprocessing include the removal of initial frames to ensure equilibration of the T1-weighted (T<sub>1</sub>w) signal and normalization of voxel time series by dividing by the mean across time of each voxel. The fMRI preprocessing pipeline started with a within-volume head motion estimation and correction by computing rigid body transformations between the first time point and each subsequent one. Scans were further processed for image distortions resulting from B0 field inhomogeneity, within-voxel field gradients and gradient nonlinearities. Isotropic resampling (2.4 mm) was performed to align fMRI volumes across each participant, and a registration matrix was computed with the T1w image. Estimates of task-related activation strength were computed at the individual level using an AFNI's 3dDeconvolve<sup>67</sup>, which implemented a general linear model (GLM) applied to each voxel's time series with additional nuisance regressors and motion estimates. Hemodynamic response functions are modeled with two parameters using a gamma variate basis function plus its temporal derivative (using AFNI's 'SPMG' option within 3dDeconvolve). Fast oscillatory signals within the motion estimates related to respiration, between 0.31 and 0.043 Hz, were temporally filtered with an infinite impulse response filter. FD was then calculated from the filtered motion estimates, and frames with an FD > 0.9 mm were censored. Preprocessed time courses were sampled onto the cortical surface for each individual participant and then registered to the standard FreeSurfer surface atlas (fsaverage). After projecting to the surface, the data were smoothed along the cortical surface (5 mm). Voxels containing cortical gray matter were projected onto the surface by sampling values 1 mm from the gray/white boundary into cortical gray matter at each vertex (using FreeSurfer's mri\_vol2surf with 'white' surface, '-projdist 1' option and default 'nearest' interpolation). Average beta coefficients and standard errors were then computed for each of the two runs of each task and for each participant, weighted by the nominal d.f. (number of frames remaining after motion censoring minus number of model parameters). Data used in the current study were derived from the data included in the ABCD data release 2.0.1 and included GLM beta coefficients and s.e.m. (calculated from the ratio of the beta and *t* statistic) calculated for each voxel and vertex. The full details of the task fMRI quality control and processing pipelines were previously described<sup>51,56</sup>.

Task models included stimulus timing for each condition and linear contrasts of conditions<sup>56</sup>. For MID and SST analyses, events were modeled as instantaneous. The EN-back task was programmed as a block design. The SST model included regressors for successful Go trials ('Correct Go'), failed Go trials ('Incorrect Go'), successful Stop trials ('Correct Stop') and failed Stop trials ('Incorrect Stop'), creating contrasts of interest correct Stop versus correct Go and incorrect Stop versus correct Go. The EN-back model included separate regressors for the 0-back faces, 2-back faces, 0-back places and 2-back places conditions; the contrasts of interest were 0-back versus fixation, 2-back versus fixation, 2-back versus 0-back, faces versus places, negative versus neutral faces and positive versus neutral faces. The MID model contained separate regressors for the different anticipation periods (large and small rewards or losses and no incentive (neutral) trials) and large and small win and loss feedback. MID-computed contrasts of interest were large reward versus neutral anticipation, small reward versus neutral anticipation, large loss versus neutral anticipation, small loss versus neutral anticipation, reward positive versus negative feedback and loss positive versus negative feedback.

**Behavioral task performance.** Poor performance on the SST leading to exclusion was determined by the following criteria: fewer than 150 Go trials, less than 60% correct on Go trials, incorrect Go trials greater than 30%, late Go trials (across correct and incorrect trials) greater than 30%, no response on Go trials greater than 30%, fewer than 30 Stop trials and Stop trial accuracy lower than 20% or

greater than 80%. The SST used an adaptive algorithm to achieve a 50% success rate. To accomplish this, the onset between the Go and Stop signal was varied based on individual performance. The adaptive algorithm allowed for calculation of the SSRT (the time required to inhibit the motor response<sup>57</sup>), which was used as the performance variable in analyses assessing individual differences in response inhibition ability. The SSRT was computed by subtracting the median SSD of all stop trials from the *n*th percentile Go reaction time, where *n* represents the percentage of successful inhibitions (for details on the theoretical underpinnings for this estimation, see Logan and Cowan<sup>58</sup>). Participants with an SSRT < 50 ms were excluded from the analysis.

For the EN-back task, *D'* was computed for both the 2-back and 0-back conditions by calculating each participant's hit rate, the proportion of targets for which the participant correctly indicated a match, and false alarm rate, the proportion of non-targets for which the participant incorrectly indicated a match or did not respond. The hit and false alarm rates were then *z* transformed. *D'* was calculated as the *z*-transformed hit rate minus the *z*-transformed false alarm rate. *D'* for the post-scan recognition memory test was also calculated for each participant in the EN-back fMRI sample as the *z*-transformed hit rate minus the *z*-transformed false alarm rate. Children were excluded from the analyses if *D'* was less than 0.

The MID task used an adaptive algorithm to maintain accuracy at 60%. To be included in the analysis, across the two runs, children had to have at least four events for each trial type, including positive and negative feedback.

**Statistical Analyses. Task activation maps.** The permutation analysis of linear models (PALM)'s GLM (<https://fsl.fmrib.ox.ac.uk/fsl/fslwiki/PALM/>) was used to generate cortical and subcortical task-specific functional activation maps, contrasting the fMRI beta weights against zero, with age (months), sex, scanner serial number, race, puberty and highest parent education included as nuisance covariates. Scanner serial number and ethnicity were entered as dummy-coded variables. All covariates were demeaned. The calculations accommodated the non-independence of the participants by incorporating information on sibling status into the exchangeability blocks of the permutation analyses. Cohen's *d* effect sizes were computed for each voxel/vertex as the mean of the residualized betas of the contrast divided by the s.d. of the residualized betas:

$$\text{Cohen's } d = \frac{\text{Mean (residualized betas)}}{\text{s.d. (residualized betas)}}$$

Thus, a Cohen's *d* effect size of 1 indicates that the mean beta weight differs from zero by 1 s.d. A threshold of  $d \geq 0.2$  was applied to the task activation maps in Figs. 3–6.

Participants with one or two siblings raise the issue of having dependent and independent participants in the analyses and implies that the data are not homoscedastic, that is, all observations do not share the same variance as there are three variance groups determined by family information (0, 1 or 2 siblings). To account for family dependence and adjust the Cohen's *d* values accordingly, we computed first, for each task, a *t* statistic map using permutation analyses ( $N = 100,000$ ) with the same covariates mentioned above. Next, we repeated the same permutation analysis after adding sibling status as a dummy-coded variable (each family received a unique value shared by the siblings of that family) implemented with PALM's exchangeability blocks structure<sup>69</sup> consisting of two columns, with each column indicating a deeper level of dependence (that is a unique dummy-coding system where indices on one level indicate how the unique subindices of the next level should be shuffled). This restricts the shuffling to only occur among the observations that share the same family index, that is, within block only. In this kind of permutation, variances are estimated for each block, and the Aspin–Welch *v* statistics that are robust to heteroscedasticity are computed instead of *t* statistics for each voxel/vertex. Finally, cortical and subcortical Cohen's *d* maps are weighted by the *t* statistic/*v* statistic ratio to generate another set of Cohen's *d* maps adjusted for family information. Only the latter maps are reported in the results.

To get an estimate of interindividual variation in activation maps, beta weights were extracted from relevant task-specific ROIs known to show robust task-specific activation. These ROIs included the bilateral IFG for the SST, bilateral dlPFC for the EN-back task and bilateral AI for the MID task. To create the IFG ROI, we combined the pars orbitalis, triangularis and opercularis parcels from the *aparc2009* FreeSurfer atlas<sup>70</sup>. To create the dlPFC ROI, we combined the bilateral middle frontal gyrus and the inferior frontal sulcus parcels from the same atlas.

**Performance correlations.** To assess the sensitivity of activation patterns to individual differences in behavioral performance, vertex and voxelwise whole-brain correlation analyses were calculated with PALM, with performance measures included as the independent variables in the design matrices and the same covariates as used above. In addition, beta weights were extracted from relevant ROIs known to show robust task-specific activation. These ROIs included bilateral inferior frontal and cingulate gyri for the SST and the bilateral dlPFC for the EN-back task. For the SST contrasts (correct Stop versus correct Go and incorrect Stop versus correct Go), Pearson's correlation coefficients were computed

between beta weights and SSRT measures. For the 0-back versus fixation and 2-back versus fixation contrasts of the EN-back task, whole-brain Pearson's correlation coefficients were computed between beta weights and  $D'$  measures derived from the 0-back and 2-back conditions, respectively. For the MID task, as its individualized adaptive algorithm does not yield a suitable performance measure directly assessing sensitivity to reward,

we went beyond the task performance measures (used with the SST and EN-back tasks) to search for correlates. We describe the relationship between MID activation and several measures assessing sensitivity to reward in Supplementary Note 6.

**Group-level spatial reproducibility.** To assess the spatial reproducibility of group activation maps and performance correlation maps (for the SST and EN-back task), we calculated the vertexwise/voxelwise correlation between a 'gold standard' map and independent samples of varying sizes. First, we split the participants into two equally sized independent groups, stratified by sex and scanner. Separately for each of the two groups, we calculated residualized beta weights according to a linear regression model fit on the following demeaned variables: age, sex, scanner serial number, race, puberty score and highest parent education. One group was designated the gold standard from which we calculated a single group activation map by computing the Cohen's  $d$  measure of effect size from all its participants in addition to Pearson's correlation coefficients between beta weights and performance measures. In the second group, we sampled random subsets, from  $n=2$  to  $n=2,500$  with 2,000 repetitions at each size, and generated a Cohen's  $d$  activation map. Each subset was sampled from the entire second group. We calculated vertex/voxelwise Pearson's correlation coefficients between each of these generated activation maps and the independent gold standard activation map. Average correlations by sample size were generated by computing the mean correlation over the 2,000 repetitions at each size. These calculations were applied to both cortical vertices and subcortical voxels. Python 3 was used to perform this analysis. The Python 3 codes are available in the 'Supplementary Software' linked to the article.

**Reporting Summary.** Further information on research design is available in the Nature Research Reporting Summary linked to this article.

## Data availability

The ABCD Study anonymized data, including all assessment domains, are released annually to the research community. Information on how to access ABCD data through the NDA is available on the ABCD Study data-sharing webpage: [https://abcdstudy.org/scientists\\_data\\_sharing.html](https://abcdstudy.org/scientists_data_sharing.html). Instructions on how to create an NDA study are available at <https://nda.nih.gov/training/modules/study.html>. The ABCD data repository grows and changes over time.

The ABCD data used in this report came from <https://doi.org/10.1515/1520620>. DOIs can be found at <https://doi.org/10.1515/1520620>. The ABCD data used in this report also came from the fast-track data release. The raw data are available at [https://nda.nih.gov/edit\\_collection.html?id=2573](https://nda.nih.gov/edit_collection.html?id=2573). Activation maps and spatial reproducibility data are available in Supplementary Data 1 and 2, respectively.

## Code availability

The Python codes used to compute reproducibility curves undertaken as part of this study and that generate the figures are openly available in the Supplementary Data and at [https://github.com/sahahn/ABCD\\_Consortium\\_Analysis](https://github.com/sahahn/ABCD_Consortium_Analysis). The following additional software packages used for this study are freely and openly available: PALM (v.alpha116), <https://fsl.fmrib.ox.ac.uk/fsl/fslwiki/PALM/>.

## References

- Paus, T. *Population Neuroscience*. (Springer, 2013).
- Garavan, H. et al. Recruiting the ABCD sample: design considerations and procedures. *Dev. Cogn. Neurosci.* **32**, 16–22 (2018).
- Petersen, A. C., Crockett, L., Richards, M. & Boxer, A. A self-report measure of pubertal status: reliability, validity, and initial norms. *J. Youth Adolesc.* **17**, 117–133 (1988).
- Glasser, M. F. et al. A multi-modal parcellation of human cerebral cortex. *Nature* **536**, 171–178 (2016).
- Hagler, D. J. et al. Image processing and analysis methods for the Adolescent Brain Cognitive Development Study. *Neuroimage* **202**, 116091 (2019).
- Logan, G. D., Schachar, R. J. & Tannock, R. Impulsivity and inhibitory control. *Psychol. Sci.* **8**, 60–64 (1997).
- Cohen, A. O., Conley, M. I., Dellarco, D. V. & Casey, B. J. The impact of emotional cues on short-term and long-term memory during adolescence. In *Proc. Society for Neuroscience, San Diego, CA* (2016).
- Hoehl, S., Brauer, J., Brasse, G., Striano, T. & Friederici, A. D. Children's processing of emotions expressed by peers and adults: an fMRI study. *Soc. Neurosci.* **5**, 543–559 (2010).
- Marusak, H. A., Carré, J. M. & Thomason, M. E. The stimuli drive the response: an fMRI study of youth processing adult or child emotional face stimuli. *Neuroimage* **83**, 679–689 (2013).

- Tottenham, N. et al. The NimStim set of facial expressions: judgments from untrained research participants. *Psychiatry Res.* **168**, 242–249 (2009).
- Conley, M. I. et al. The racially diverse affective expression (RADIATE) face stimulus set. *Psychiatry Res.* **270**, 1059–1067 (2018).
- Kanwisher, N. Neural events and perceptual awareness. *Cognition* **79**, 89–113 (2001).
- Park, S. & Chun, M. M. Different roles of the parahippocampal place area (PPA) and retrosplenial cortex (RSC) in panoramic scene perception. *Neuroimage* **47**, 1747–1756 (2009).
- Knutson, B., Westdorp, A., Kaiser, E. & Hommer, D. fMRI visualization of brain activity during a monetary incentive delay task. *Neuroimage* **12**, 20–27 (2000).
- Yau, W.-Y. W. et al. Nucleus accumbens response to incentive stimuli anticipation in children of alcoholics: relationships with precursive behavioral risk and lifetime alcohol use. *J. Neurosci.* **32**, 2544–2551 (2012).
- Cox, R. W. AFNI: software for analysis and visualization of functional magnetic resonance neuroimages. *Comput. Biomed. Res.* **29**, 162–173 (1996).
- Logan, G. D. & Cowan, W. B. On the ability to inhibit thought and action: a theory of an act of control. *Psychol. Rev.* **91**, 295 (1984).
- Winkler, A. M., Webster, M. A., Vidaurre, D., Nichols, T. E. & Smith, S. M. Multi-level block permutation. *Neuroimage* **123**, 253–268 (2015).
- Destrieux, C., Fischl, B., Dale, A. & Halgren, E. Automatic parcellation of human cortical gyri and sulci using standard anatomical nomenclature. *Neuroimage* **53**, 1–15 (2010).

## Acknowledgements

Data used in the preparation of this article were obtained from the ABCD Study (<https://abcdstudy.org>) held in the NDA. This is a multisite, longitudinal study designed to recruit more than 10,000 children ages 9–10 years old and follow them over 10 years into early adulthood. The ABCD study is supported by the National Institutes of Health and additional federal partners under award numbers U01DA041048, U01DA050989, U01DA051016, U01DA041022, U01DA051018, U01DA051037, U01DA050987, U01DA041174, U01DA041106, U01DA041117, U01DA041028, U01DA041134, U01DA050988, U01DA051039, U01DA041156, U01DA041025, U01DA041120, U01DA051038, U01DA041148, U01DA041093, U01DA041089, U24DA041123 and U24DA041147. A full list of supporters is available at <https://abcdstudy.org/federal-partners.html>. A listing of participating sites and a complete listing of the study investigators can be found at [https://abcdstudy.org/consortium\\_members/](https://abcdstudy.org/consortium_members/). ABCD consortium investigators designed and implemented the study and/or provided data, but did not necessarily participate in the analysis or writing of this report. Most ABCD research sites rely on a central Institutional Review Board (IRB) at the University of California, San Diego, for the ethical review and approval of the research protocol, with a few sites obtaining local IRB approval. The views expressed in this manuscript are those of the authors and do not necessarily reflect the official views of the National Institutes of Health, the Department of Health and Human Services, the US federal government or ABCD consortium investigators. Computations were performed on the Vermont Advanced Computing Core supported, in part, by NSF award number OAC-1827314. A. Ivanciu and E. Pearson helped with the submission process. G. Dowling was substantially involved in all of the cited grants, M. Lopez and J. Matochik were substantially involved in U24DA041147, and S. Grant and A. Noronha were substantially involved in U24DA041123, consistent with their roles as Scientific Officers. All other Federal representatives contributed to the interpretation of the data and participated in the preparation, review and approval of the manuscript, consistent with their roles on the ABCD Federal Partners Group. The views and opinions expressed in this manuscript are those of the authors only and do not necessarily represent the views, official policy or position of the U.S. Department of Health and Human Services or any of its affiliated institutions or agencies.

## Author contributions

B.C., N.A., S.Hahn and H.P.G. performed neuroimaging data processing and analysis. B.C., M.M.O., A. Potter and H.P.G. prepared the manuscript. B.C., S. Adise, D.J.H., M.D.C., S. Hatton, A.M.D. and H.P.G. performed the quality control and preprocessing of behavioral and neuroimaging data. B.C., N.A., S. Hahn, S. Adise, M.M.O., A.C.J., D.K.Y., H.L., A. Ivanciu, M.D.A., J.D., S.M., J.L., M.I., D.J.H., M.D.C., S. Hatton, A.A., L. Aguinaldo, L. Ahonen, W.A., A.P.A., J.A., S. Avenevoli, D. Babcock, K.B., F.C.B., M.T.B., D.M.B., H.B., A.B., J.M.B., D. Blachman-Demmer, M.B., R.B., S.Y.B., F.B., S.B., F.J.C., V.C., B.J.C., L.C., D.B.C., C.C., R.T.C., K.C., R.C., L.B.C., S.C., R. K. Dagher, A.M.D., M.D., R. Delcarmen-Wiggins, A.S.D., E.K.D., N.U.D., G.J.D., S.E., T.M.E., D.A.F., C.C.F., E.F., S.W.F., P.F., J.J.F., E.G.F., N.P.F., S.F., B.F.F., A.G., D.G.G., J. Giedd, M. Glantz, P.G., J. Godino, M. Gonzalez, R.G., S.G., K.M.G., F.H., M.P.H., S. Hawes, A.C.H., S. Heeringa, M.M. Heitzeg, R.H., M.M. Herting, J.M.H., J.K.H., C.H., E.H., K.H., R.S.H., M.A.H., L.W.H., W.G.I., M.A.I., O.I., A. Isaiah, S.I., J.J., R.J., B.J., T.J., N.R.K., A. Kaufmann, B. Kelley, B. Kit, A. Ksinan, J.K., A.R. Laird, C. Larson, K. LeBlanc, C. Lessov-Schlagger, N.L., D.A.L., K. Lisdahl, A.R. Little, M. Lopez, M. Luciana, B.L., P.A.M., H.H.M., C. Makowski, A.T.M., M.J.M., J.M., B.D.M., E.M., I.M., G.M., A.M., C. Mulford, P.M., B.J.N., M.C.N., G.N., A. Nencka, A. Noronha, S.J.N., C.E.P., V.P., M.P.P., W.E.P., D. Pfefferbaum, C.P., A. Prescott, D. Prouty, L.I.P., N.R., K.M.R., G.R., P.F.R., M.C.R., P.R., M.R., M.D.R., M.J.R., M. Sanchez, C. Schrida, D.S., J. Schulenberg, K.J.S., C. Sheth, P.D.S., W.K.S.,

E.R.S., N.S., M. Spittel, L.M.S., C. Sripada, J. Steinberg, C. Striley, M.T.S., J.T., S.F.T., W.T., R.L.T., K.A.U., S.V., N.E.W., R.W., S.W., B.A.W., O.D.W., A. Wilbur, D. Wing, D. Wolff-Hughes, R.Y., D.A.Y., R.A.Z., A. Potter and H.P.G. contributed to the study design, collected the data and reviewed the manuscript.

### Competing interests

The authors declare no competing interests.

### Additional information

**Supplementary information** The online version contains supplementary material available at <https://doi.org/10.1038/s41593-021-00867-9>.

**Correspondence and requests for materials** should be addressed to B.C. or H.P.G.

**Peer review information** *Nature Neuroscience* thanks Sarah-Jayne Blakemore, Iroise Dumontheil, and Chandan Vaidya for their contribution to the peer review of this work.

**Reprints and permissions information** is available at [www.nature.com/reprints](http://www.nature.com/reprints).

## Reporting Summary

Nature Research wishes to improve the reproducibility of the work that we publish. This form provides structure for consistency and transparency in reporting. For further information on Nature Research policies, see [Authors & Referees](#) and the [Editorial Policy Checklist](#).

### Statistics

For all statistical analyses, confirm that the following items are present in the figure legend, table legend, main text, or Methods section.

- |                                     |  |
|-------------------------------------|--|
| n/a                                 | Confirmed  |
| <input type="checkbox"/>            | <input checked="" type="checkbox"/> The exact sample size ( $n$ ) for each experimental group/condition, given as a discrete number and unit of measurement  |
| <input checked="" type="checkbox"/> | <input type="checkbox"/> A statement on whether measurements were taken from distinct samples or whether the same sample was measured repeatedly   |
| <input type="checkbox"/>            | <input checked="" type="checkbox"/> The statistical test(s) used AND whether they are one- or two-sided<br><i>Only common tests should be described solely by name; describe more complex techniques in the Methods section.</i>   |
| <input type="checkbox"/>            | <input checked="" type="checkbox"/> A description of all covariates tested   |
| <input checked="" type="checkbox"/> | <input type="checkbox"/> A description of any assumptions or corrections, such as tests of normality and adjustment for multiple comparisons   |
| <input type="checkbox"/>            | <input checked="" type="checkbox"/> A full description of the statistical parameters including central tendency (e.g. means) or other basic estimates (e.g. regression coefficient) AND variation (e.g. standard deviation) or associated estimates of uncertainty (e.g. confidence intervals) |
| <input type="checkbox"/>            | <input checked="" type="checkbox"/> For null hypothesis testing, the test statistic (e.g. $F$ , $t$ , $r$ ) with confidence intervals, effect sizes, degrees of freedom and $P$ value noted<br><i>Give <math>P</math> values as exact values whenever suitable.</i>                            |
| <input checked="" type="checkbox"/> | <input type="checkbox"/> For Bayesian analysis, information on the choice of priors and Markov chain Monte Carlo settings  |
| <input checked="" type="checkbox"/> | <input type="checkbox"/> For hierarchical and complex designs, identification of the appropriate level for tests and full reporting of outcomes  |
| <input type="checkbox"/>            | <input checked="" type="checkbox"/> Estimates of effect sizes (e.g. Cohen's $d$ , Pearson's $r$ ), indicating how they were calculated   |

Our web collection on [statistics for biologists](#) contains articles on many of the points above.

### Software and code

Policy information about [availability of computer code](#)

- |                 |  |
|-----------------|--|
| Data collection | No software was used for data collection.  |
| Data analysis   | Software used in the analyses are Permutation Analysis of Linear Models (PALM; version alpha116) and Python 3. An R script to remove Philips fMRI data from tabulated data is available at <a href="https://github.com/ABCD-STUDY/fMRI-cleanup">https://github.com/ABCD-STUDY/fMRI-cleanup</a> . |

For manuscripts utilizing custom algorithms or software that are central to the research but not yet described in published literature, software must be made available to editors/reviewers. We strongly encourage code deposition in a community repository (e.g. GitHub). See the Nature Research [guidelines for submitting code & software](#) for further information.

### Data

Policy information about [availability of data](#)

All manuscripts must include a [data availability statement](#). This statement should provide the following information, where applicable:

- Accession codes, unique identifiers, or web links for publicly available datasets
- A list of figures that have associated raw data
- A description of any restrictions on data availability

The ABCD Study anonymized data including all assessment domains is released annually to the research community. Information on how to access ABCD data through the NIMH Data Archive (NDA) is available on the ABCD study data sharing webpage: [https://abcdstudy.org/scientists\\_data\\_sharing.html](https://abcdstudy.org/scientists_data_sharing.html). Instructions on how to create an NDA study are available at <https://nda.nih.gov/training/modules/study.html>. The ABCD data repository grows and changes over time. The ABCD data used in this report came from 10.15154/1520620. DOIs can be found at <https://dx.doi.org/10.15154/1520620>. The ABCD data used in this report also came from the fast-track data release. The raw data are available at [https://nda.nih.gov/edit\\_collection.html?id=2573](https://nda.nih.gov/edit_collection.html?id=2573).



## Field-specific reporting

Please select the one below that is the best fit for your research. If you are not sure, read the appropriate sections before making your selection.

☒ Life sciences ☐ Behavioural & social sciences ☐ Ecological, evolutionary & environmental sciences

For a reference copy of the document with all sections, see [nature.com/documents/nr-reporting-summary-flat.pdf](https://www.nature.com/documents/nr-reporting-summary-flat.pdf)

## Life sciences study design

All studies must disclose on these points even when the disclosure is negative.

Sample size	The Adolescent Brain Cognitive Development Study ( <a href="http://www.ABCDstudy.org">www.ABCDstudy.org</a> ) is a 10-year longitudinal study of 11,880 children recruited at ages 9 and 10. This is the largest neuroimaging study ever conducted in the US. No sample size calculation was performed. Sample size included all participants with data surviving the exclusion criteria detailed below.
Data exclusions	participants were included if they had 1) two fMRI runs per task, 2) cortical vertex and subcortical voxel data available at the time of analysis, 3) hemispheric mean beta-weights within two standard deviations of the sample mean for each task, 4) at least 200 degrees of freedom over the two scan runs, 5) had mean framewise displacement < 0.9 mm for both runs, 6) met task-specific performance criteria, and 7) had complete information for covariates of interest (age, sex, scanner serial number, race, puberty (Peterson et al. 1988) and highest parent education).
Replication	we report the spatial reproducibility of activation patterns by assessing between-group vertex/voxelwise correlations of BOLD activation as a function of sample size n. We calculated vertex/voxelwise Pearson's correlation coefficients between each of these generated activation maps and the independent "gold standard" activation map. Average correlations by sample size were generated by computing the mean correlation over the 2,000 repetitions at each size.
Randomization	The ABCD study is a single cohort, observational and longitudinal design that has not randomization of participants to groups. The analyses in the current study used Permutation Analysis of Linear Models general linear model ( <a href="https://fsl.fmrib.ox.ac.uk/fsl/fslwiki/PALM/">https://fsl.fmrib.ox.ac.uk/fsl/fslwiki/PALM/</a> ) to generate cortical and subcortical task-specific functional activation maps, contrasting the fMRI beta weights versus zero, with age (months), sex, scanner serial number, race, puberty and highest parent education included as nuisance covariates. The calculations accommodated the non-independence of the participants by incorporating information on sibling status into the exchangeability blocks of the permutation analyses.
Blinding	We used a single cohort longitudinal design and group analyses include all participant meeting inclusion criteria. Therefore, blinding was not relevant in our analyses.

## Reporting for specific materials, systems and methods

We require information from authors about some types of materials, experimental systems and methods used in many studies. Here, indicate whether each material, system or method listed is relevant to your study. If you are not sure if a list item applies to your research, read the appropriate section before selecting a response.

### Materials & experimental systems

### Methods

n/a	Involved in the study	n/a	Involved in the study
<input checked="" type="checkbox"/>	<input type="checkbox"/> Antibodies	<input checked="" type="checkbox"/>	<input type="checkbox"/> ChIP-seq
<input checked="" type="checkbox"/>	<input type="checkbox"/> Eukaryotic cell lines	<input checked="" type="checkbox"/>	<input type="checkbox"/> Flow cytometry
<input checked="" type="checkbox"/>	<input type="checkbox"/> Palaeontology	<input type="checkbox"/>	<input checked="" type="checkbox"/> MRI-based neuroimaging
<input checked="" type="checkbox"/>	<input type="checkbox"/> Animals and other organisms		
<input type="checkbox"/>	<input checked="" type="checkbox"/> Human research participants		
<input checked="" type="checkbox"/>	<input type="checkbox"/> Clinical data		

## Human research participants

Policy information about [studies involving human research participants](#)

Population characteristics	ABCD adopted a population neuroscience approach to recruitment by employing epidemiologically informed procedures to ensure demographic variation in its sample that would mirror the variation in the US population of 9- and 10-year-olds. Samples used in the analyses were 50% males and 50% females overall.
Recruitment	The ABCD sample was largely recruited through public, private, and charter elementary schools. A probability sampling of schools was conducted within the defined catchment areas of the study's nationally distributed set of 21 recruitment sites.
Ethics oversight	The ABCD Study uses a single IRB that acts as the IRB of record for 19 of the 21 sites. This single IRB is located at the UCSD HRPP (Human Research Protections Program). Non-reliant sites obtained local IRB approvals.

Note that full information on the approval of the study protocol must also be provided in the manuscript.

# Magnetic resonance imaging

## Experimental design

### Design type

Event-related and block design task fMRI

### Design specifications

The Stop Signal Task (SST) had two runs. Each had 180 trials, of which 30 were “Stop” trials, yielding a total of 60 “Stop” trials and 300 “Go” trials. Each trial lasted 1sec. The time between the “go” and “stop” signals (the Stop-Signal Delay; SSD) varied dynamically based on a participant’s success on the prior trial so as to achieve a 50% success rate (starting at 50 msec, the SSD increased by 50 msec if the participant successfully stopped on the previous trial, and decreased by 50 msec if he/she responded).

The EN-back consisted of two runs, each containing eight blocks of trials and four 15 sec periods containing just a fixation cross. Blocks contained 10 trials lasting 2.5 sec each and were preceded by a 2.5 sec instruction screen indicating the condition for the upcoming block. Of the 10 trials in each block, 2 were targets, 2–3 were non-target lures, and the remainder were non-lures (i.e., stimuli only presented once). There are 160 trials in total with 96 unique stimuli of 4 different stimulus types (24 unique stimuli per type).

The Monetary Incentive Delay (MID) task consists of twelve optimized trial orders of the task (2 runs each). Each run consists of 50 contiguous trials (10 per trial type) presented in pseudorandom order and lasts 5:42. The specific sequence of each trial was as follows: participants saw a cue denoting the trial type (2s), with “win” trials shown in a pink circle, “lose” trials shown in a yellow square, and “neutral” trials shown in a blue triangle. Then, participants viewed a fixation cross of jittered duration (1.5–4 sec), followed by a signal to respond, denoted by a black shape that corresponded to the trial type. The duration of the response signal varied between trials (0.15–0.5 sec), with the initial response target duration determined by the participant’s performance during a practice session prior to scanning.

### Behavioral performance measures

Task models included stimulus timing for each condition and linear contrasts of conditions. The SST model included regressors for successful go trials (“Correct Go”), failed go trials (“Incorrect Go”), successful stop trials (“Correct Stop”), and failed stop trials (“Incorrect Stop”), creating contrasts of interest Correct Stop vs Correct Go and Incorrect Stop vs Correct Go. The EN-back model included separate regressors for the 0-back faces, 2-back faces, 0-back places, and 2-back places conditions; the contrasts of interest were 0-back vs. Fixation, 2-back vs. Fixation, 2-back vs. 0-back, Faces vs. Places, negative vs neutral faces and positive vs neutral faces. The MID model contained separate regressors for the different anticipation periods (large and small rewards or losses and no incentive [“neutral”] trials) and large and small win and loss feedback. MID computed contrasts of interest were Large Reward versus Neutral Anticipation, small Reward versus Neutral Anticipation, Large Loss versus Neutral Anticipation, small Loss versus Neutral Anticipation, Reward Positive versus Negative Feedback, Loss Positive versus Negative Feedback.

The SST used an adaptive algorithm to achieve a 50% success rate. To accomplish this, the onset between the GO and STOP signal was varied based on individual performance. Poor performance on the SST was determined by: fewer than 150 GO trials, less than 60% correct on GO trials, incorrect GO trials greater than 30%, late GO trials (across correct and incorrect trials) greater than 30%, no response on GO trials greater than 30%, fewer than 30 STOP trials, and STOP trial accuracy lower than 20% or greater than 80%. The adaptive algorithm allowed for calculation of the Stop Signal Reaction Time (SSRT, the time required to inhibit the motor response; 2), which was used as the performance variable in analyses assessing individual differences in response inhibition ability. The SSRT was computed by subtracting the median stop signal delay of all successful stop trials from the nth percentile go reaction time, where n represents the percentage of successful inhibitions. Children with SSRT less than 50 msec were excluded from the analysis (n=3).

For the EN-back, D’ was computed for both the 2-back and 0-back conditions by calculating each participant’s hit rate, the proportion of targets for which the participant correctly indicated a match, and false alarm rate, the proportion of non-targets for which the participant incorrectly indicated a match or did not respond. The hit and false alarm rates were then z-transformed. D’ was calculated as the z-transformed hit rate minus the z-transformed false alarm rate. Children were excluded from the analyses if D’ was less than 0.

The MID task used an adaptive algorithm to maintain accuracy at 60%. To be included in the analysis, across the two runs, children had to have at least four events for each trial type, including positive and negative feedback.

## Acquisition

### Imaging type(s)

Functional MRI

### Field strength

3 Tesla

### Sequence & imaging parameters

High spatial and temporal resolution simultaneous multi-slice (SMS)/multiband EPI task-based fMRI scans, with fast integrated distortion correction, are acquired to examine functional activity. For Siemens and GE scanners, the scanning parameters were: matrix of 90 x 90, 60 slices, FOV= 216 x 216, TE/TR (msec) = 800/30, flip angle= 52 degrees, and

resolution (mm) = 2.4 x 2.4 x 2.4.

Area of acquisition

Whole brain

Diffusion MRI

☐ Used☒ Not used

## Preprocessing

Preprocessing software

We used a collection of processing steps contained within the Multi-Modal Processing Stream (MMPS), a software package developed and maintained in-house at the Center for Multimodal Imaging and Genetics (CMIG) at the University of California, San Diego (UCSD) that provides large-scale, standardized processing and analysis of multimodality neuroimaging data on Linux workstations and compute clusters. For ABCD Release 2.0.1, MMPS version 251 was used. This toolbox contains primarily MATLAB functions, as well as python, sh, and csh scripts, and C++ compiled executables and relies upon a number of publicly available neuroimaging software packages, including FreeSurfer (Fischl, 2012), Analysis of Functional NeuroImages (AFNI) (Cox, 1996), and FMRIB Software Library (FSL) (Jenkinson et al., 2012; Smith et al., 2004). Estimates of task-related activation strength are computed at the individual subject level using a general linear model (GLM) implemented in AFNI's 3dDeconvolve (Cox, 1996). Hemodynamic response functions are modelled with two parameters using a gamma variate basis function plus its temporal derivative (using AFNI's 'SPMG' option within 3dDeconvolve). Task models include stimulus timing for each condition and linear contrasts of conditions. For MID and SST analyses, events are modelled as instantaneous; for EN-back, the duration of cues (~3s) and trial blocks (~24s) are modelled as square waves convolved with the two parameter gamma basis function (i.e., block duration specified when using AFNI's 'SPMG' option). Outputs include GLM beta coefficients and standard errors of the mean (SEM; calculated from the ratio of the beta and t-statistic) calculated for each voxel and vertex). Cortical surface reconstruction and subcortical segmentation are performed using FreeSurfer v5.3.

Normalization

For vertex-wise analyses, surfaces were nonlinearly registered surface atlas based on cortical folding patterns with FreeSurfer. For voxel-wise analyses, T1w images were registered to atlas using affine and nonlinear registration with FSL's flirt and fnirt, respectively.

Normalization template

The template for surface-based registration was standard FreeSurfer average brain surface spherical atlas. 5 mm FWHM surface-based smoothing was applied before resampling to atlas. The Template for voxel-wise registration was FSL's T1\_2\_MNI152\_2mm. 5 mm FWHM volume-based smoothing was applied before resampling to atlas.

Noise and artifact removal

Baseline and quadratic trends in the time-series data are included in the analysis. Motion estimates and their derivatives are also included as regressors (Power et al., 2014). Estimated motion time courses used for regression and censoring are temporally filtered using an infinite impulse response (IIR) notch filter to attenuate signals in the range of 0.31 - 0.43 Hz. This frequency range corresponds to empirically observed oscillatory signals in motion estimates linked to respiration and the dynamic changes in magnetic susceptibility due to lung movement in the range of 18.6 - 25.7 respirations / minute. With the removal of these fast oscillations linked to respiration, the filtered motion estimates and FD values more accurately reflect actual head motion (Fair et al., 2018).

Volume censoring

Time points with FD greater than 0.9 mm were censored (Siegel et al., 2014).

## Statistical modeling &amp; inference

Model type and settings

Mass univariate and Pearson correlation analyses were carried-out with the nuisance covariates mentioned above included in the design matrices

Effect(s) tested

- Cohen's d effect size for task-fMRI BOLD activation  
- Pearson's Correlation coefficients between task-fMRI BOLD and performance measures

Specify type of analysis:

☐ Whole brain☐ ROI-based☒ Both

Anatomical location(s)

Anatomical Destrieux cortical atlas was used

Statistic type for inference  
(See [Eklund et al. 2016](#))

For this descriptive study only effect sizes were reported. No statistic inference was applied.

Correction

See above.

## Models &amp; analysis

n/a | Involved in the study

☒ ☐ Functional and/or effective connectivity☒ ☐ Graph analysis☒ ☐ Multivariate modeling or predictive analysis